

Brain4FMs: A Benchmark of Foundation Models for Electrical Brain Signals

Fanqi Shen
shenfanqi@zju.edu.cn
Zhejiang University
Hangzhou, Zhejiang, China

Junru Chen
jrchen_cali@zju.edu.cn
Zhejiang University
Hangzhou, Zhejiang, China

Li Meng
limeng.braindecoder@gmail.com
Shanghai Institute of Microsystem
and Information Technology, CAS
Shanghai, China

Enhong Yang
yeh1115@zju.edu.cn
Zhejiang University
Hangzhou, Zhejiang, China

Xiaoran Pan
panxiaoran@zju.edu.cn
Zhejiang University
Hangzhou, Zhejiang, China

Jiahe Li
jiaheli@zju.edu.cn
Zhejiang University
Hangzhou, Zhejiang, China

Zhizhang Yuan
zhizhangyuan@zju.edu.cn
Zhejiang University
Hangzhou, Zhejiang, China

Yang Yang
yangya@zju.edu.cn
Zhejiang University
Hangzhou, Zhejiang, China

Abstract

Brain Foundation Models (BFMs) are transforming neuroscience by enabling scalable and transferable learning from neural signals, advancing both clinical diagnostics and cutting-edge neuroscience exploration. Their emergence is powered by large-scale clinical recordings, particularly electroencephalography (EEG) and intracranial EEG, which provide rich temporal and spatial representations of brain dynamics. However, despite their rapid proliferation, the field lacks a unified understanding of existing methodologies and a standardized evaluation framework. To fill this gap, we map the benchmark design space along two axes: (i) from the model perspective, we organize BFMs under a self-supervised learning (SSL) taxonomy; and (ii) from the dataset perspective, we summarize common downstream tasks and curate representative public datasets across clinical and human-centric neurotechnology applications. Building on this consolidation, we introduce Brain4FMs, an open evaluation platform with plug-and-play interfaces that integrates 15 representative BFMs and 18 public datasets. It enables standardized comparisons and analysis of how pretraining data, SSL strategies, and architectures affect generalization and downstream performance, guiding more accurate and transferable BFMs. The code is available at <https://anonymous.4open.science/r/Brain4FMs-85B8>.

CCS Concepts

• Computing methodologies → Machine learning; • Applied computing → Health informatics.

Keywords

Brain Foundation Model, Electroencephalography, Self-Supervised Learning, Benchmarking and Evaluation

1 Introduction

Neuroscience is fundamental to understanding the brain and translating insights into societal impact. Beyond supporting clinical

advances in neurological disease detection [86] and sleep staging [2], the study of neural mechanisms drives paradigms in human-technology interaction, including neural communication [79] and affective computing [118]. Electroencephalography (EEG) and intracranial EEG (iEEG) provide millisecond temporal resolution, high fidelity and direct measurements of neural electrical activity.

Deep learning has emerged as a powerful tool for neural signal analysis, with architectures such as CNNs, LSTMs, and GNNs achieving promising results in decoding tasks [27, 55, 83]. However, reliance on small, task-specific labeled datasets limits generalization, given the high cost of annotation and inter-subject variability. To overcome these limitations, self-supervised learning (SSL) leverages unlabeled neural data for representation learning [34]. This shift parallels advances in Natural Language Processing (NLP) [21] and Computer Vision (CV) [24], where large-scale pretraining enabled foundation models. A similar transition is emerging in neuroscience, with Brain Foundation Models (BFMs) serving as universal encoders that learn robust representations across subjects and support efficient adaptation to downstream tasks (Figure 1).

Recent surveys review BFMs from pretraining, architectural, and application perspectives [3, 51, 56, 120]. However, a unified SSL-centric, formulation-based perspective for systematically organizing methods and enabling principled comparison remains lacking. Existing benchmarks are also limited, as they either focus on specific tasks [20, 61] or lack comprehensive coverage of datasets and models [101, 104]. To bridge these gaps, we propose a unified operator-based formulation for SSL pretraining (Figure 1a), and introduce a cross-task benchmark with cross-subject finetuning for standardized evaluation. The main contributions of this paper are:

- 1) **Unified Taxonomy of SSL Mechanisms.** We present an up-to-date, SSL-centric taxonomy for BFMs by abstracting methods into a unified objective and categorizing them into three paradigms, enabling systematic comparison of learning mechanisms.
- 2) **Extensive Benchmark for BFMs Evaluation.** We construct an open benchmark covering 11 downstream tasks across 18 EEG and

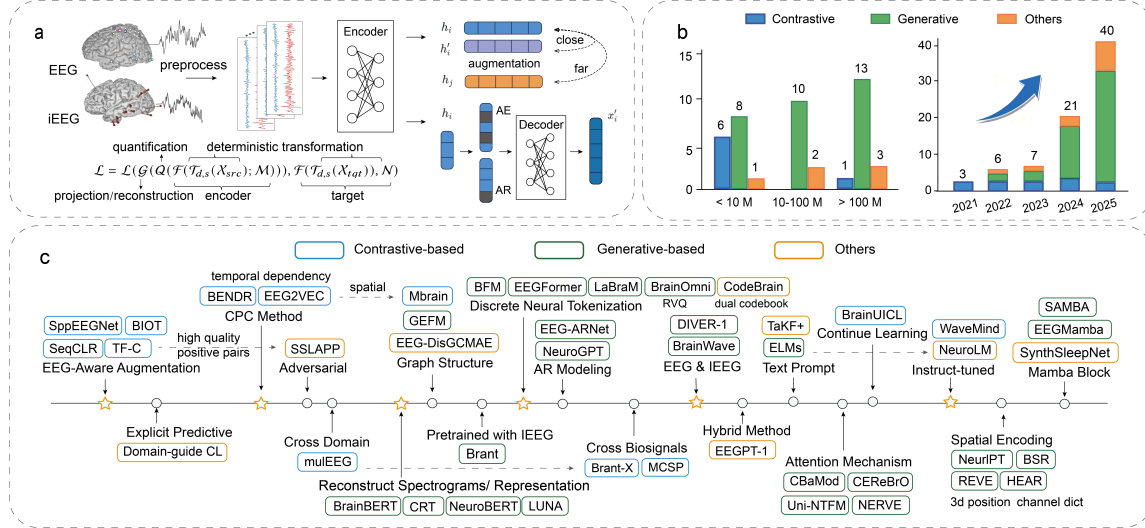


Figure 1: Overview of BFM. (a) A unified pretraining pipeline. EEG/iEEG recordings are preprocessed, encoded into latent representations, and optimized under different SSL paradigms. (b) Model scale statistics. Parameter-size buckets by training paradigm are shown for the reported subset, using each model’s maximum parameter count, alongside yearly model counts under the same grouping. (c) Timeline-style family tree of representative BFM from 2021 to 2025, organized by paradigm and annotated with major methodological shifts.

iEEG public datasets, enabling consistent comparison through a standardized preprocessing and evaluation pipeline.

3) **Systematic Analysis.** We perform a comprehensive study on 15 BFM, analyzing how pretraining data, training strategies, and architectures affect generalization and downstream performance.

2 Model Taxonomy

EEG and iEEG are naturally modeled as multivariate time series. We denote a recording as $X \in \mathbb{R}^{C \times N}$, where C is the number of channels and $N = f_s \times t$ is the number of samples over duration t at sampling rate f_s . For electrode-wise representations, let $\epsilon \subseteq \{1, \dots, C\}$ be a subset of electrodes with $E_\epsilon = |\epsilon|$. The corresponding multivariate time series is $x^\epsilon \in \mathbb{R}^{E_\epsilon \times N}$. We categorize pretraining pipelines into patch-level and sequence-level formulations. In patch-level modeling, the raw signal X is partitioned along the temporal dimension into k non-overlapping windows of length $w = \frac{N}{k}$. Objectives are defined at the patch granularity, and patches are typically treated as exchangeable tokens. Sequence-level modeling preserves the temporal structure and treats the input as an ordered sequence.

SSL derives training signals from the data, enabling pretraining without manual annotations. Most SSL methods can be viewed as optimizing an objective constructed from transformations and prediction modules applied to the input signal. We form two sets from input, a source set X_{src} and a target set X_{tgt} . An encoder $\mathcal{F}(\cdot)$ maps the input to a d -dimensional latent representation, followed by an optional module $\mathcal{G}(\cdot)$ that serves either as a decoder for reconstruction or as a prediction or alignment head. Under this formulation, SSL methods can be expressed with a unified objective:

$$\mathcal{L}_{sum} = \mathcal{L}(\mathcal{G}(\mathcal{F}(\mathcal{T}_{d,s}(X_{src}), \mathcal{M})), \mathcal{F}(\mathcal{T}_{d,s}(X_{tgt})), \mathcal{N}) \quad (1)$$

Here, $\mathcal{T}_{d,s} = \Phi_d \circ a_s$ denotes a deterministic transform composed of domain mapping Φ_d and augmentation a_s . The tokenizer $Q(\cdot)$ discretizes continuous latent representations. And \mathcal{M} denotes a

masking operator, while \mathcal{N} is the negative set when contrastive objectives are employed. Based on this formulation, we categorize BFM pretraining strategies into three SSL paradigms. We focus on the underlying learning mechanisms in this section, and defer detailed model instantiations and developments to Appendix A.

2.1 Contrastive-based Methods

Contrastive-based SSL defines learning objectives by comparing representations of paired inputs and contrasting them against a set of negatives. This paradigm can be expressed as:

$$\mathcal{L}_C = \mathcal{L}(z_1, z_2, \mathcal{N}) \quad (2)$$

where $z_1 = \mathcal{F}_1(\mathcal{T}_{d,s}(X_{src}, \mathcal{M}))$ and $z_2 = \mathcal{F}_2(\mathcal{T}_{d,s}(X_{tgt}))$, $\mathcal{F}_1(\cdot)$ produces a query representation from the causal context while $\mathcal{F}_2(\cdot)$ generates the target embedding from a future segment. The projection head $\mathcal{G}(\cdot)$ maps representations into a latent space. The loss contrasts the positive pair (z_1, z_2) with negatives \mathcal{N} , promoting alignment of matched pairs and separation from mismatches.

2.1.1 Augmentation Contrast. Augmentation-based method constructs positive pairs by applying transformations to the same input. Given an input $x_i \in X_{src}$, two augmented views are generated as $x_i^1 = \mathcal{T}_s(x_i)$ and $x_i^2 = \mathcal{T}_s(x_i)$, where \mathcal{T}_s is an augmentation operator designed to preserve neural semantics. The positive pair is (x_i^1, x_i^2) , while negatives \mathcal{N} are obtained from samples $\mathcal{T}_s(x_j)$ with $x_j \in X_{src}$ and $j \neq i$. For neural signals, effective augmentations must retain physiologically meaningful patterns rather than introducing arbitrary perturbations. Beyond standard time-domain perturbations (e.g., jittering, scaling, and temporal shifts), work explores frequency-domain transformations that selectively suppress or inject spectral components [58, 115] as well as view construction for multichannel recordings [71, 105]. Recent work enforces subject-level consistency via same-subject representation alignment [94].

2.1.2 Contrastive Predictive Coding. Contrastive Predictive Coding (CPC) [80] formulates contrastive objectives over ordered representations. In CPC-based pretraining, an encoder produces a context representation $c_i = \mathcal{F}_1(\mathcal{T}_{d,s}(X_{src}, \mathcal{M}))$, where $\mathcal{F}_1(\cdot)$ encodes observations and aggregates past information into a contextual state. Conditioned on c_i , the model extracts a target representation $z_i = \mathcal{F}_2(\mathcal{T}_{d,s}(X_{tgt}))$ from a future segment. Projection operator $\mathcal{G}(\cdot)$ maps c_i into a latent space, where a contrastive objective aligns the context with future representation z_i while contrasting it against negatives. CPC-based BFM range from sequence-level modeling [49, 122] to spatio-temporal architectures [13].

2.1.3 Cross-modal Contrast. Cross-modal contrastive learning aligns representations derived from complementary views or modalities that reflect the same neural state. In EEG/iEEG, two views are constructed via the composite transform $\mathcal{T}(\cdot)$ and assigned as $x_{m_1} \in X_{src}$ and $x_{m_2} \in X_{tgt}$. Features are extracted using modality-specific encoders $\mathcal{F}_1(\cdot)$ and $\mathcal{F}_2(\cdot)$. Unidirectional alignment is adopted by freezing the target branch with a stop-gradient operator $sg[\cdot]$. Cross-modal BFM range from contrasting multiple EEG/iEEG-derived views [50, 95] to aligning heterogeneous biosignals [87, 111], and further to EEG/iEEG–multimodal alignment [26, 28].

2.2 Generative-based Methods

Generative-based SSL formulates pretraining objectives by reconstructing or predicting structured targets from transformed inputs, avoiding explicit pair construction and negative sampling [113]. This paradigm has become increasingly prevalent in recent BFMs. Given a transformed input $\mathcal{T}_d(x)$, an encoder $\mathcal{F}_{\theta_1}(\cdot)$ produces a continuous latent representation $z_i = \mathcal{F}_{\theta_1}(\mathcal{T}_d(x_i))$ where $x_i \in X_{src}$. A learnable codebook $Q_{\theta_3}(\cdot)$ discretizes z_i into a latent embedding, which is then processed by a decoder $\mathcal{G}_{\theta_2}(\cdot)$ to reconstruct a target view or predict future content. The objective is defined as:

$$\mathcal{L}_G = \mathcal{L}(\mathcal{G}_{\theta_2}(Q_{\theta_3}(\mathcal{F}_{\theta_1}(\mathcal{T}_d(x_i), \mathcal{M}))), \mathcal{F}_{\theta_1}(\mathcal{T}_d(x_i))) \quad (3)$$

By minimizing the reconstruction or prediction loss, the model learns latent representations that retain information necessary to recover the underlying signal structure.

2.2.1 Autoregressive-based. Autoregressive (AR) modeling learns representations by causal prediction over ordered sequences [44]. In BFMs, neural signals are cast as token sequences, and learning proceeds via next-token prediction from past context. Given an index i and a prediction window of length k , future tokens are predicted from the causal context $x_{\leq i} \in X_{src}$ under a causal constraint. AR-based BFMs progress from patch-level prediction with GPT-style decoders [19, 63] to richer spatio-temporal modeling for cross-channel dependencies [70, 98, 108, 119]. Recent work further incorporates prompt-based conditioning for in-context learning [59].

2.2.2 Autoencoder-based. Autoencoder-based methods learn representations by reconstructing transformed inputs through an encoder–decoder architecture [68] and are widely used in BFMs [47]. An encoder $\mathcal{F}_{\theta_1}(\cdot)$ maps the input x_i or an optional transformed view $\mathcal{T}_d(x_i)$ into a latent code, and then decoded by $\mathcal{G}_{\theta_2}(\cdot)$ to reconstruct a target view. The reconstruction objective encourages the latent space to preserve information required for signal recovery.

AE-based BFMs evolve from masked reconstruction in the time domain [18, 35, 41, 91] to domain-aware masking strategies operating in spectral or latent space [10, 90, 99, 100, 107, 113]. To better handle multi-electrode recordings, models incorporate spatial inductive biases through channel dictionaries, positional encodings, or graph-structured connectivity, enabling modeling of cross-channel topology [17, 25, 81, 93]. Transformer backbones are increasingly adopted to capture long-range temporal dependencies and spatial interactions [23, 60, 92], and masked learning has been further scaled to iEEG and large-population datasets [31, 90, 107, 112].

Recent BFMs further discretize EEG/iEEG signals into token sequences via codebook quantization, bridging autoencoding with token-based generative modeling. This line of work progresses from direct temporal quantization [9] to pretrained VQ-VAE tokenizers [16, 39, 40], and toward more structured codebooks, including time–frequency dual tokenizers [67], topology-aware hierarchical VQ-VAE variants [106], and residual codebooks [10]. Codebooks are objective-agnostic and can also pair with non-AE objectives.

2.3 Other Advanced Methods

Beyond the SSL paradigms discussed above, BFMs explore explicit predictive objectives, hybrid formulations, and post-SSL instruction tuning. These methods extend the pretraining framework along dimensions of supervision, objective design, and task alignment.

2.3.1 Explicit Predictive-based. Explicit predictive-based methods learn representations by predicting predefined, interpretable attributes of the signal derived from $\mathcal{T}_{d,s}(\cdot)$, such as temporal order, channel configuration, or future patterns. These pretext tasks impose supervised-like objectives grounded in intrinsic signal structure. The general form of the loss is given by:

$$\mathcal{L}_{ep} = \mathcal{L}(\mathcal{G}_{\theta_2}(\mathcal{F}_{\theta_1}(X_{src}, \mathcal{M})), \mathcal{T}_{d,s}(x)) \quad (4)$$

where $\mathcal{G}_{\theta_2}(\cdot)$ denotes a task-specific prediction head, and \mathcal{M} is an optional masking operator. In EEG/iEEG applications, predictive targets are often designed to reflect neurophysiological properties [43, 89]. Such objectives rely on predefined predictive targets and are therefore tied to specific assumptions about signal structure.

2.3.2 Hybrid-based. Hybrid SSL combines multiple self-supervised objectives within a unified framework to exploit complementary learning signals [97]. Recent BFMs couple contrastive objectives with generative modeling to jointly capture cross-view consistency and signal structure [14, 52, 54, 91, 96]. Other approaches integrate reconstruction with autoregressive prediction to model both signal structure and temporal dynamics [38, 106], and may further incorporate adversarial objectives for domain-aware alignment [39, 53].

2.3.3 Instruction-tuned. Instruction tuning is not a self-supervised paradigm, but is typically applied after SSL pretraining as a supervised alignment stage to support multi-task decoding. In this setting, EEG/iEEG features are mapped to LLM-compatible tokens through an adapter or tokenizer Q_{θ_2} , and a pretrained language model \mathcal{G}_{θ_3} generates task outputs y conditioned on prompts \mathcal{P} :

$$\mathcal{L}_{it} = \mathcal{L}(\mathcal{G}_{\theta_2}(Q_{\theta_3}(\mathcal{F}_{\theta_1}(X_{src})), \mathcal{P}), y) \quad (5)$$

Existing designs mainly differ in the choice of tokenization strategies, alignment schemes, and prompt formulations [14, 37, 39, 109].

3 Benchmark

To promote standardized and reproducible evaluation, we introduce Brain4FMs, a comprehensive benchmark for BFM-based electrical brain signal classification. It integrates 15 BFMs and 18 public datasets for systematic cross-task assessment, and provides plug-and-play interfaces for adding new models and datasets.

3.1 Pipeline

The benchmark focuses on classification tasks, which aims to divide the input electrical brain signal samples $X = x_1, x_2, \dots, x_n$ into pre-defined categories $C = c_1, c_2, \dots, c_m$, where x_i represents the i -th sample, m is the number of categories, and c'_i is predicted labels. The evaluation pipeline is organized into two stages: data preprocessing, followed by model finetuning and evaluation (Figure 2b). Preprocessing includes bandpass and notch filtering, downsampling, event-aligned window segmentation, channel selection, and per-channel z-score normalization. Then, use BFMs with pre-trained weights as the main backbone model M to extract hidden features z_i , and fine-tune the model with task-specific classifiers Cl_i :

$$z_i = M(x_i); c'_i = Cl_i(z_i) \quad (6)$$

We adopt a cross-subject leave-subjects-out protocol with train/valid/test splits of approximately 3:1:1, ensuring no data leakage. This setup enforces generalization to unseen subjects and is critical for clinical applicability in neuroscience [107]. Models are evaluated via group-wise cross-validation, with results reported as the mean performance across all test folds for reliable comparison.

As summarized in Table 1, Brain4FMs includes 15 BFMs spanning diverse pretraining strategies and evaluates them systematically across datasets. All models are tested under identical protocols, enabling fair and comprehensive comparison across neural decoding tasks and supporting robustness assessment across subjects. The included BFMs are chosen from accepted or highly cited works with public code and pretrained weights.

Table 1: Overview of benchmark models, including SSL strategies, BFMs parameters, pretraining data modalities and feature domain.

Name	Strategy	Param	Modality	Domain
Contrastive-based Method				
SppEEGNet [58]	Aug.	138 K	EEG	time
BIOT [105]	Aug.	3.19 M	EEG	time, frequency
Bendr [49]	CPC	3.97 M	EEG	time, frequency
MBrain [13]	CPC	8.34 M	EEG/iEEG	time, frequency, space
Generative-based Method				
Brant [112]	AE	196.10 M	iEEG	time, frequency, space
BFM [9]	AE	708.96 M	EEG	time
Brainbert [90]	AE	43.18 M	iEEG	time, frequency
CBraMod [92]	AE	4.88 M	EEG	time, frequency, space
NeuroGPT [19]	AR	79.62 M	EEG	time, frequency
LaBraM [40]	AE	5.80 M	EEG	time, frequency, space
BrainWave [107]	AE	102.13 M	EEG+iEEG	time, frequency, space
REVE [81]	AE	69.19 M	EEG	time, space
BrainOmni [103]	AE	32.71 M	EEG	time, frequency, space
Other Advanced Method				
EEGPT-1 [91]	G & C	51.04 M	EEG	time, space
NeuroLM [39]	G & Adv.	169.60 M	EEG	time, frequency

3.2 Dataset Construction

Brain4FMs presents a comprehensive benchmark covering 18 public datasets across 11 tasks, grouped into four categories: disease diagnosis, sleep staging, communication [114], and affective computing. Table 2 summarizes widely used datasets that support cross-subject evaluation and comprise EEG or iEEG recordings collected across diverse experimental settings. Most datasets are disjoint from the pretraining corpora of the evaluated BFMs. Pretraining sources, limited overlap, and dataset statistics are provided in Appendix B.

3.2.1 Disease Diagnosis. Neurological disorders are a major global health burden, representing the leading cause of disability and the second leading cause of death worldwide [57]. To support clinically relevant evaluation, Brain4FMs groups disease diagnosis tasks, including Epilepsy, drug-resistant epilepsy (DRE), Parkinson’s Disease (PD), Depression, Major Depression Disorder (MDD), Schizophrenia Disease (SD), Attention Deficit Hyperactivity Disorder (ADHD) and Alzheimer’s Disease (AD). These tasks align with real clinical objectives, featuring cross-subject splits and clinically grounded labels to enable robust, generalizable evaluation.

3.2.2 Sleep Staging. Sleep staging supports the diagnosis and treatment of sleep disorders. Manual scoring of overnight recordings is labor-intensive and time-consuming, motivating automatic sleep stage classification [2]. The task requires modeling long-duration signals and capturing rich time-frequency structure, making robust long-range temporal modeling essential.

3.2.3 Communication. Communication maps neural activity to external outputs, enabling intent expression for users with severe motor impairments. Typical tasks include Motor Imagery (MI), Motor Execution (ME) and decoding speech or semantic intent, translating brain signals into symbolic outputs for spelling, typing, or command selection.

3.2.4 Affective Computing. Affective computing infers internal emotional and cognitive states from EEG or iEEG. Core tasks include emotion recognition and mental workload estimation (MW), which rely on time-frequency and spatial patterns to capture arousal, valence, and cognitive demand across diverse settings.

3.3 Centralized Benchmarking Results

We evaluate 22 downstream classification tasks from 18 public datasets, as some datasets contain multiple subtasks. Standard metrics are reported, including Accuracy, AUROC, F1, F2, and Cohen’s κ , with full results provided in Appendix D. In our tables, C/G/O/Adv. denote Contrastive/Generative/Other/Adversarial methods, while Aug./Hyb./CB indicate augmentation/hybrid/codebook approaches. Performance varies significantly across tasks, with no single BFMs consistently outperforming others. To interpret these differences and inform future development, we organize our analysis along a typical pipeline, from pretraining data and SSL strategies to model design with a focus on spatial or frequency structure and discrete representations. This motivates the five questions below:

- Q1: How do data composition and modality affect BFMs performance?
- Q2: How do SSL strategies correlate with cross-task performance?
- Q3: Do BFMs learn task-relevant spatial structure?
- Q4: How is frequency information represented in BFMs across tasks?

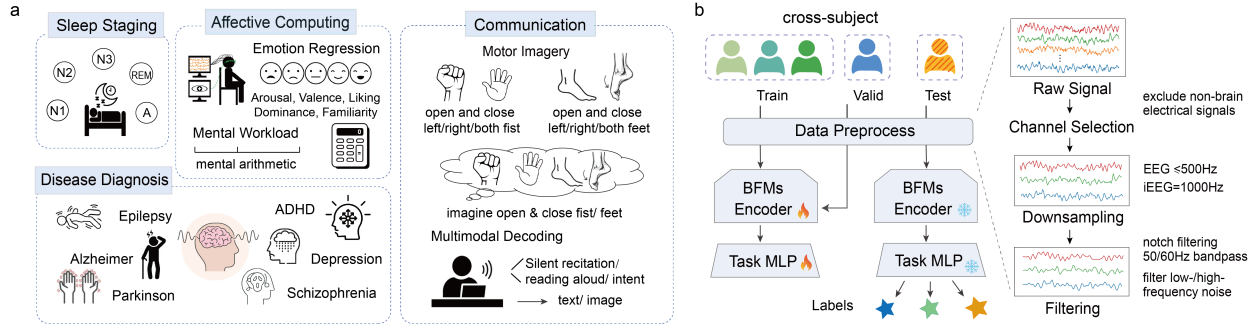


Figure 2: Overview of benchmark pipeline. (a) Data acquisition scenarios covering sleep staging, affective computing, disease diagnosis, and communication. (b) Evaluation under cross-subject and cross-validation protocols, with a standardized EEG/iEEG preprocessing pipeline.

Q5: Do codebook discretization strategies benefit BFM?

3.3.1 Q1: How do data composition and modality affect BFM performance? From a data perspective, a primary factor is the modality of the pretraining corpus. On epilepsy datasets (Table 3), iEEG-pretrained models tend to perform better on iEEG cohorts, while EEG-pretrained models favor EEG datasets. For example, Brant, pretrained on iEEG, achieves strong performance on MAYO and FNUSA with high AUROC and Accuracy, but degrades markedly on CHBMIT, revealing pronounced modality dependence. By contrast, BrainWave, pretrained jointly on EEG and iEEG, remains robust across settings, consistent with improved tolerance to domain shift.

Task-specific supervised baselines are provided as reference points: SPaRCNet [42] for epilepsy, DeprNet [85] for depression, CCNSE [55] for sleep staging, and MSCARNet [4] for communication and affective computing. For completeness, we also report their best results on ADHD, AD, and PD as supervised references rather than task-optimized baselines. Regarding epilepsy and sleep

staging benchmarks, BFM exhibit stronger cross-subject transfer under unified evaluation protocols. Supervised baselines can be competitive but typically outperform only a subset of BFM. In epilepsy, SPaRCNet outperforms SppEEGNet, NeuroLM, and BFM in both AUROC and accuracy, while most BFM still achieve higher overall performance. CCNSE achieves moderate AUROC but low accuracy, indicating limited calibration. In contrast, on depression datasets such as MDD-64, DeprNet remains a strong baseline but is surpassed by several BFM (e.g., REVE, BrainOmni, and BrainWave). Overall, these results indicate that large-scale pretraining yields more transferable representations than task-specific supervised training in most clinical diagnosis settings.

Communication and affective computing remain challenging for cross-subject generalization [65] due to strong non-stationarity and large cross-subject/inter-session variability (Table 5). The BCI-tailored supervised baseline MSCARNet shows stronger cross-subject transfer than most BFM. Although several BFM show improvements on benchmarks (e.g., NeuroGPT), their overall transfer performance on concept decoding and emotion recognition remains limited. In contrast, MI and MW tasks are more separable, enabling models such as REVE and NeuroGPT to achieve higher Accuracy and AUROC, and BrainOmni performs strongly on EEGMMIDB.

Table 2: Public datasets used in the benchmark, including signal type, number of subjects (Sub.), and dataset category (Cat.), where H denotes healthy subjects.

Name	Signal	Task	Subject	Cat.
CHBMIT [30]	EEG	Epilepsy	23 sub.	2
MAYO [75]	iEEG	DRE	25 sub.	2
FNUSA [75]	iEEG	DRE	14 sub.	2
Dep-BDI [36]	EEG	Depression	122 sub.	2
MDD-64 [73]	EEG	MDD	30H, 43MDD	2
SD-28 [102]	EEG	SD	28 sub.	2
UCSD [84]	EEG	PD	31H, 15PD	2
ADFD [69]	EEG	AD	88 sub.	2
ADHD_Adult [7]	EEG	ADHD	42H 37ADHD	2
ADHD_Child [72]	EEG	ADHD	60H 61ADHD	2
ISRU [46]	EEG	Sleep Stage	100 sub.	5
SleepEDFx [45]	EEG	Sleep Stage	44 sub.	5
DEAP [48]	EEG	Emotion Recognition	32 sub.	4
SEED-IV [117]	EEG	Emotion Recognition	15 sub.	4
EEGMat [123]	EEG	MW	36 sub.	2
EEGMMIDB [29]	EEG	MI & ME	109 sub.	4
BCI-2a [11]	EEG	MI	9 sub.	4
Chisco [116]	EEG	Concept Classification	5 sub.	39

Table 3: Primary performance metrics of BFM on epilepsy datasets. We show a representative subset across method types, C/G/O/SL denote contrastive/generative/other/supervised methods.

Type	Method	MAYO		FNUSA		CHBMIT	
		AUROC	Acc	AUROC	Acc	AUROC	Acc
C	MBrain	.92±.04	.92±.02	.91±.08	.87±.08	.71±.03	.73±.06
	BIOT	.90±.07	.88±.05	.87±.07	.83±.08	.56±.08	.29±.05
	SppEEGNet	.56±.03	.75±.05	.64±.08	.67±.05	.43±.05	.60±.06
G	BrainWave	.98±.01	.93±.02	.92±.05	.89±.06	.90±.03	.80±.12
	BrainBERT	.97±.01	.94±.01	.90±.04	.89±.04	.78±.06	.75±.10
	LaBraM	.96±.02	.93±.02	.89±.08	.82±.10	.75±.10	.73±.10
	Brant	.92±.03	.82±.12	.87±.12	.84±.07	.55±.05	.70±.01
	BrainOmni	.91±.06	.90±.02	.88±.07	.84±.05	.74±.13	.67±.19
	BFM	.81±.08	.68±.08	.78±.12	.69±.11	.74±.075	.72±.03
	EEGPT	.92±.03	.90±.03	.90±.04	.84±.06	.71±.09	.67±.11
O	NeuroLM	.64±.09	.72±.16	.64±.14	.72±.17	.67±.06	.54±.20
	SPaRCNet	.83±.10	.83±.08	.85±.10	.82±.11	.61±.10	.66±.05

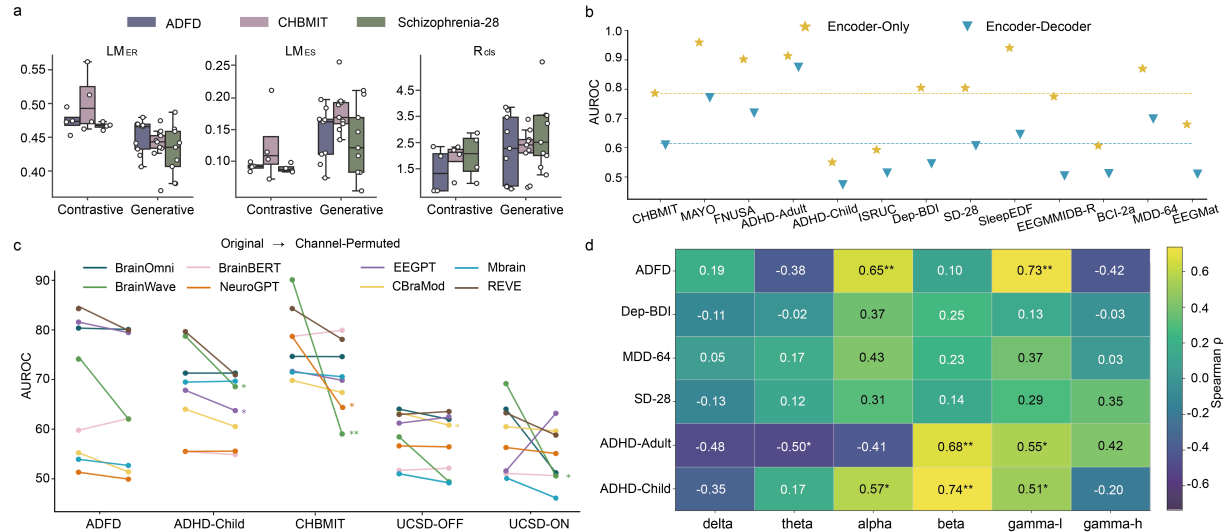


Figure 3: Supplemental analyses. (a) Box plots of decision-boundary diagnostics ($q=0.10$) comparing contrastive and generative models on cross-subject tasks. (b) AUROC of NeuroGPT variants across tasks. (c) Slopegraph of AUROC changes from original to channel-permuted, comparing spatially strong and weak models. (d) Heatmap of Spearman's rank correlation between band-wise predictability and model performance rankings across tasks. Points in (a-c) denote n-fold cross-validation means; asterisks in (c-d) indicate $^*(p<0.05)$ and $^{**}(p<0.001)$.

These results suggest that current BFM capture motor-related neural patterns more reliably than higher-level affective or communicative semantics. Notably, even models pretrained with emotion-related data (e.g., NeuroLM) may perform competitively in within-subject settings but still struggle to generalize across subjects.

3.3.2 Q2: How do SSL strategies correlate with cross-task performance? A consistent paradigm-associated gap is observed: contrastive-based BFM tend to underperform generative-based ones on most downstream tasks in the benchmark (e.g., seizure detection, AD, SD, and PD). This gap cannot be attributed solely by the SSL objective, as the models also differ in pretraining data, architecture, and scale. To probe the potential role of SSL, decision-boundary diagnostics are conducted on three representative datasets, comparing contrastive and generative models through analyses of their

embedding spaces and classifier boundaries. Given predicted probabilities $p(x)$ and the margin $m(x) = p_i(x) - p_j(x)$, the boundary region is defined as $\mathcal{B}_q = x \mid m(x) < Q_q(m)$, where $Q_q(\cdot)$ denotes the q -quantile of the margin distribution. Relative trends remain stable for $q \in 0.05, 0.10, 0.20$, $q = 0.10$ is therefore used in the main text, with full sensitivity analyses reported in Appendix E. The error-at-boundary proportion LM_{ER} and the boundary-in-errors proportion LM_{ES} are then computed as follows:

$$LM_{ER} = \frac{|\{x \in \mathcal{B}_q : \hat{y}(x) \neq y(x)\}|}{|\mathcal{B}_q|}, \quad LM_{ES} = \frac{|\{x \in \mathcal{B}_q : \hat{y}(x) \neq y(x)\}|}{|\{x : \hat{y}(x) \neq y(x)\}|}$$

To quantify embedding cluster structure, the class-separation ratio R_{cls} is adopted, defined as the average inter-class distance divided by the average intra-class distance. Higher values indicate more compact clusters and greater separation between classes.

Across all three datasets, a consistent pattern emerges. Contrastive models show higher LM_{ER} than generative models, indicating more frequent misclassification in the low-margin boundary region and weaker discrimination near the decision boundary. Generative models, in turn, achieve markedly higher R_{cls} , reflecting tighter within-class clusters and larger inter-class separation, corresponding to a more separable latent geometry. Notably, despite higher boundary-region error rates, contrastive models often present lower LM_{ES} , indicating that their errors are less concentrated near the boundary. This suggests that generative models primarily fail on ambiguous borderline samples, whereas contrastive models incur errors farther from the boundary, consistent with less stable global geometry and decision surfaces. Results are summarized in Figure 3a, with full quantitative values reported in Appendix E.

Contrastive BFM are analyzed by distinguishing augmentation methods from CPC approaches. CPC-based models show stronger robustness and transferability across clinically relevant tasks, with

Table 4: AUROC and Accuracy (Acc) on ME, MW, emotion recognition and concept decoding datasets. Chisco-R results are reported with three decimal places for clarity.

Model	EEGMMIDB-R		EEGMat		DEAP		Chisco-R	
	AUROC	Acc	AUROC	Acc	AUROC	Acc	AUROC	Acc
MBrain	.52±.01	.26±.01	.68±.06	.75±.02	.51±.05	.42±.04	.038±.004	
BIOT	.50±.01	.25±.01	.59±.08	.27±.01	.50±.03	.30±.06	.037±.003	
REVE	.82±.00	.59±.01	.78±.09	.75±.08	.50±.05	.26±.05	.026±.003	
NeuroGPT-E	.77±.02	.54±.02	.70±.04	.73±.04	.49±.01	.42±.03	.047±.004	
NeuroGPT-D	.50±.00	.25±.00	.51±.06	.73±.01	.51±.03	.44±.04	.048±.003	
BrainOmni	.74±.01	.49±.01	.68±.07	.60±.07	.45±.03	.22±.03	.030±.009	
CBraMod	.57±.01	.30±.02	.63±.06	.72±.04	.51±.01	.19±.02	.025±.009	
LaBraM	.55±.02	.28±.02	.71±.03	.68±.04	.51±.02	.29±.04	.033±.007	
BrainBERT	.50±.01	.25±.00	.61±.07	.67±.06	.52±.02	.23±.02	.032±.005	
BrainWave	.50±.01	.25±.01	.66±.06	.51±.20	.51±.03	.27±.07	.029±.005	
MSCARNet	.80±.01	.57±.01	.59±.06	.74±.01	.51±.04	.39±.03	.047±.004	

Table 5: Primary performance metrics on disease disorder and sleep staging. We show a subset of BFM across method types and SL^\dagger denotes dataset-specific supervised baselines, MSCARNet for AD/PD/SD, SPaRCNet for ADHD, DeprNet for MDD, and CCNSE for Sleep.

Method		ADHD-Adult		ADHD-Child		ADFD		MDD-64		SD-28		SleepEDF		UCSD-ON	
SSL	Model	AUROC	Acc												
C	MBrain	.95±.03	.92±.04	.69±.11	.63±.08	.53±.12	.50±.10	.93±.08	.87±.11	.58±.10	.58±.10	.94±.01	.79±.04	.49±.15	.46±.14
	Bendr	.62±.03	.61±.04	.53±.02	.51±.01	.52±.02	.52±.01	.78±.07	.73±.04	.49±.05	.50±.03	.91±.01	.69±.06	.51±.05	.49±.05
G	REVE	.96±.02	.91±.02	.79±.07	.71±.04	.84±.07	.77±.08	.97±.04	.88±.09	.81±.13	.75±.13	.78±.38	.63±.30	.63±.19	.56±.13
	BrainOmni	.96±.02	.91±.02	.71±.09	.62±.07	.80±.07	.71±.04	.94±.07	.85±.09	.69±.15	.69±.12	.87±.00	.63±.03	.53±.14	.49±.12
	BrainWave	.96±.03	.91±.04	.78±.04	.71±.04	.74±.05	.68±.05	.94±.03	.85±.02	.88±.07	.81±.06	.89±.02	.67±.05	.69±.20	.53±.08
	CBraMod	.95±.02	.92±.04	.64±.05	.64±.06	.55±.06	.59±.04	.90±.13	.84±.12	.54±.14	.58±.05	.93±.01	.73±.04	.60±.12	.49±.08
	LaBraM	.95±.04	.91±.04	.66±.12	.64±.08	.72±.07	.68±.05	.87±.12	.81±.11	.54±.07	.54±.04	.93±.01	.76±.04	.51±.22	.45±.11
	BrainBERT	.74±.05	.69±.05	.55±.03	.56±.03	.59±.05	.58±.05	.92±.07	.85±.07	.73±.11	.66±.15	.91±.02	.68±.07	.51±.05	.51±.06
O	EEGPT	.96±.03	.91±.04	.67±.13	.64±.10	.81±.05	.72±.05	.94±.05	.87±.08	.56±.21	.56±.11	.91±.00	.68±.03	.51±.21	.48±.17
	NeuroLM	.82±.14	.75±.07	.64±.06	.60±.05	.51±.04	.53±.03	.82±.11	.80±.06	.49±.04	.49±.05	.61±.06	.18±.04	.44±.18	.51±.18
SL^\dagger	Dataset-spec	.94±.02	.89±.03	.66±.05	.62±.03	.73±.11	.69±.08	.91±.06	.78±.04	.78±.15	.74±.09	.84±.02	.33±.04	.48±.19	.44±.08

MBrain emerging as the strongest contrastive baseline, achieving consistently higher AUROC and accuracy. Augmentation methods are not uniformly inferior; for example, BIOT remains competitive for ADHD and AD. Nevertheless, CPC approaches dominate performance on most datasets. This trend aligns with differences in training signals. Augmentation approaches rely on generic perturbations to form positive pairs, which may introduce boundary noise under high inter-subject variability. CPC instead exploits temporal continuity by segment prediction, encouraging representations that preserve physiological dynamics. MBrain integrates multi-channel CPC with a GNN to capture both spatial and long-range temporal dependencies, benefiting time-structured tasks.

Within the generative family, most BFM favor AE pretraining over AR paradigms. A plausible explanation lies in the mismatch between AR objectives and downstream EEG/iEEG classification tasks. AR models predict each step from past context, producing inherently unidirectional representations [62], whereas AE-style model aggregates bidirectional context over the entire window. Since most tasks involve global discrimination rather than sequence generation [110], such bidirectional, window-level representations are generally more suitable for feature learning. Controlled experiments on NeuroGPT further support this interpretation. Two variants are finetuned: an encoder-only model (NeuroGPT-E) and an encoder-decoder model (NeuroGPT-D). Both are evaluated across multiple downstream tasks, including epilepsy, sleep staging, MW, and MI in Figure 3b, and full results are reported in Appendix D. NeuroGPT-E consistently outperforms NeuroGPT-D, indicating that finetuning performance in brain signal classification tasks is largely driven by encoder representations, while the decoder contributes more limited gains in this setting.

3.3.3 Q3: Do BFM learn task-relevant spatial structure? Several top-performing models in our benchmark, such as BrainWave, BrainOmni, and REVE, are designed with a special structure to capture the multi-channel characteristics of EEG/iEEG signals. This motivates testing whether BFM internalize dataset-specific spatial structure during training. We therefore apply channel-permutation perturbations to the train/valid splits while keeping the test split unchanged. Spatially strong models (BrainWave, BrainOmni, CBraMod, EEGPT, MBrain, REVE) are compared with spatially weak models

(BrainBERT, NeuroGPT-E) by examining AUROC changes and assessing statistical significance using paired tests in Figure 3c. And full results are in Appendix F.

It finds that performance degradation under spatial perturbation is mainly driven by task-specific spatial dependence. We distinguish spatial heterogeneity, which captures region-specific channel statistics, from spatial topology dependence, which requires modeling relative channel organization and propagation. Channel permutation preserves per-channel temporal statistics while removing absolute channel ordering, enabling assessment of topology invariance. Epilepsy is widely regarded as a spatiotemporal network disorder involving seizure onset and propagation across cortical regions [1]. Thus, it shows strong sensitivity to spatial topology, for which channel permutation causes substantial AUROC drops. PD is characterized by region-specific spectral abnormalities [8] and pronounced spatial heterogeneity, resulting in an intermediate sensitivity to permutation. In contrast, ADHD exhibits milder sensitivity. Although its signals are often linked to frontal network dysfunction [74], performance depends less on precise channel adjacency, leading to smaller drops. For AD, where biomarkers primarily reflect global spectral statistics rather than localized cortical patterns [5], most models remain largely unaffected by channel permutation, with BrainWave as a notable exception.

Clear architectural differences in robustness are further observed. Among spatially weak models, BrainBERT does not explicitly encode channel interactions and is thus insensitive to channel permutation, whereas NeuroGPT-E degrades on some datasets. And for spatially strong models, BrainWave, which uses CNN to capture spatial information, drops on CHBMIT, ADHD-Child, and ADFD, suggesting it may rely on generic inter-channel attention rather than learning dataset-specific spatial structure. EEGPT similarly remains sensitive to channel-identity perturbations on spatially heterogeneous tasks despite implicit channel alignment. In contrast, other spatially strong models are more stable across tasks and datasets. By explicitly encoding channel topology via graph structures, spatial embeddings, or semantic spatial modeling, they encourage learning relative spatial topology rather than absolute channel indices, improving robustness to channel reconfiguration.

3.3.4 Q4: How is frequency information represented in BFM across tasks? Models reconstructing frequency-domain features (e.g., BrainWave, BrainBERT, LaBraM) demonstrate strong performance across tasks, particularly in disease diagnosis. This aligns with evidence that different frequency bands encode distinct cognitive and pathological states [12]. Compared with raw waveforms, which entangle multiple oscillatory components with noise, transformed representations make the oscillatory structure more explicit. Reconstruction in frequency domains, therefore, encourages models to capture band-structured statistics tied to neural rhythms, which may better match EEG/iEEG physiology than fitting the raw signal.

Motivated by this, we probe whether BFM encode dominant frequency bands (six bands; Figure 3d) by freezing the fine-tuned encoder and training a lightweight band-wise Power Spectral Density (PSD) head that maps embeddings to the band-specific PSD profiles via separate linear heads per band. Let $P_b(x)$ and $\hat{P}_b(x)$ denote the ground-truth and predicted PSD for band b . We measure band predictability by $r_b = \text{corr}(P_b(x), \hat{P}_b(x))$, then normalize r_b across bands to obtain each band's relative predictive strength as r_b^n , with detailed results reported in Appendix G. Finally, Spearman rank correlation and significance are computed between r_b^n and downstream performance rankings, primarily based on AUROC, to link frequency encoding with task performance.

The results show clear task-dependent patterns. In ADFD, the relative predictability of α and γ_l is significantly correlated with performance ranking. In depression tasks, correlations are uniformly weak and non-significant. In ADHD-Adult, β and γ_l show significant positive correlations, whereas θ is negatively correlated. In ADHD-Child, α , β , and γ_l are all significantly associated with performance, with β being the strongest. Across several datasets, band-wise relative predictability shows a consistent association with performance ranking. Clinically, AD is often linked to elevated δ/α and θ/α ratios [76], while ADHD studies highlight the relevance of θ/β -related markers [64]. It suggests that BFM emphasize different frequency bands across tasks, and some salient bands are task-relevant. This task-adaptive frequency emphasis may help guide improvements in downstream performance.

3.3.5 Q5: Do codebook discretization strategies benefit BFM? Discrete codebooks have recently been introduced in BFM to improve representation stability and generalization. To assess the impact of codebook design on representation usage and discriminability, three benchmark models with explicit discretization (BFM, LaBraM, BrainOmni) are analyzed. These models adopt distinct mechanisms. BFM applies the tokenizer from Chronos to discretize raw signals into token IDs. LaBraM discretizes encoder features during pre-training via a VQ-VAE but removes the codebook during finetuning. BrainOmni follows a similar paradigm but employs multi-layer residual vector quantization (RVQ). We analyze codebook behavior on the test set by characterizing token-embedding geometry, using *inter* to measure class-wise center similarity and distance ratio (*DR*) to quantify inter-intra class separation.

It observes clear design-dependent behaviors. BFM activates many tokens with high coverage and entropy, yet exhibits extremely high *inter* and low *DR*, suggesting that a generic temporal codebook favors cross-domain robustness but is hard to encode task-specific EEG/iEEG semantics. LaBraM shows sparser and

Table 6: Codebook token usage and class geometry under different settings. We report the coverage (Cov.) and entropy (Ent.) of token, mean inter-class similarity (inter), and inter-/intra-class distance ratio (DR) for BFM, fine-tuned and non-fine-tuned LaBraM (*LaBraM_{no}*), and BrainOmni with four RVQ layers.

Model	ADFD			CHBMIT			SD-28					
	Cov.	Ent.	inter	DR	Cov.	Ent.	inter	DR	Cov.	Ent.	inter	DR
BFM	.430	.868	.998	.002	.635	.838	.999	.001	.547	.853	.999	.001
BrainOmni ₁	.997	.947	.996	.007	.988	.948	.999	.001	.964	.941	.999	.002
BrainOmni ₂	.998	.891	.928	.077	.998	.950	.966	.037	.998	.982	.994	.007
BrainOmni ₃	.998	.929	.927	.076	.998	.970	.959	.043	.998	.973	.954	.049
BrainOmni ₄	.998	.946	.947	.055	.998	.988	.930	.072	.998	.972	.909	.094
LaBraM _{no}	.353	.755	.995	.006	.369	.721	.973	.038	.171	.607	.986	.022
LaBraM	.140	.694	.267	1.155	.093	.518	-.954	6.755	.043	.586	.800	.294

more preferential token usage, although its *inter* and *DR* improve over BFM, class separation remains weak, indicating that the pre-trained codebook cannot directly transfer into class-discriminative geometry for downstream tasks. In contrast, BrainOmni's hierarchical RVQ maintains high token coverage and entropy, and as the residual level deepens, *DR* tends to increase. This suggests that coarse-to-fine discretization can mitigate codebook collapse and progressively introduce more class-discriminative structure. Further, fine-tuning LaBraM's codebook results in decreased token coverage and entropy, alongside increased class separation, indicating that the codebook is able to adapt to new tasks. However, reusing discretization during finetuning still degrades downstream performance, suggesting quantization may constrain discriminative flexibility and discard fine-grained cues (Appendix H). Overall, the results in Table 6 highlight hierarchical discretization as a promising route to balance robustness and capacity for BFM.

4 Conclusion

Brain4FMs provides a unified, plug-and-play framework for analyzing BFM. We organize BFM with an SSL-centric taxonomy and evaluate 15 models on 18 public datasets under standardized cross-subject finetuning, enabling fair and reproducible comparison. Our analyses relate performance variation to key factors, including pre-training data composition, SSL strategy, and model design. Together, Brain4FMs offers a solid reference for future BFM development and supports transparent, comparable, and extensible evaluation in this rapidly evolving field. We plan to extend the benchmark with frozen-encoder, few-shot, and zero-shot settings, and to keep the open-source leaderboard up to date.

References

- [1] 2020. Ictal EEG source localization in focal epilepsy: Review and future perspectives. *Clinical Neurophysiology* 131, 11 (2020), 2600–2616.
- [2] Khalid Ali I Aboalayon, Miad Faezipour, Wafaa S Almuhammadi, and Saeid Moslehpoor. 2016. Sleep stage classification using EEG signal analysis: a comprehensive survey and new investigation. *Entropy* 18, 9 (2016), 272.
- [3] Hamdi Altaheri, Fakhri Karray, Md Milon Islam, SM Raju, and Amir-Hossein Karimi. 2025. Bridging Brain with Foundation Models through Self-Supervised Learning. *arXiv preprint arXiv:2506.16009* (2025).
- [4] Danilo Avola, Luigi Cinque, Angelo Di Mambro, Romeo Lanzino, Daniele Pannone, and Francesco Scarcello. 2024. Multi-stream 1d CNN for EEG motor imagery classification of limbs activation. *IEEE Access* 12 (2024), 83940–83951.
- [5] Claudio Babiloni, Raffaele Ferri, Davide V Moretti, Andrea Strambi, Giuliano Binetti, Gloria Dal Forno, Florinda Ferreri, Bartolo Lanuzza, Claudio Bonato,

Flavio Nobili, et al. 2004. Abnormal fronto-parietal coupling of brain rhythms in mild Alzheimer's disease: A multicentric EEG study. *European Journal of Neuroscience* 19, 9 (2004), 2583–2590.

[6] Alexei Baevski, Yuhao Zhou, Abdelrahman Mohamed, and Michael Auli. 2020. wav2vec 2.0: A framework for self-supervised learning of speech representations. *Advances in neural information processing systems* 33 (2020), 12449–12460.

[7] Ghassam Sadeghi Bajestani, Shima Abedian, Fatemeh Makhlooughi, Motahareh Raoufatabar, and Hamid Saeedi. 2023. A dataset of eeg signals from adults with adhd and healthy controls: Resting state, cognitive function, and sound listening paradigm. *Mendeley Data* (2023).

[8] Jacopo Barone and Holly E Rossiter. 2021. Understanding the role of sensorimotor beta oscillations. *Frontiers in systems neuroscience* 15 (2021), 655886.

[9] Mohammad Javad Darvishi Bayazi, Hena Ghonia, Roland Riachi, Bruno Arisitunha, Arian Khorasani, Md Rifat Arefin, Amin Darabi, Guillaume Dumas, and Irina Rish. [n. d.]. General-Purpose Brain Foundation Models for Time-Series Neuroimaging Data. In *NeurIPS Workshop on Time Series in the Age of Large Models*.

[10] Ruggiero G Bettinardi, Mohamed Rahmouni, and Ulysse Gimenez. 2025. BioSerenity-E1: a self-supervised EEG model for medical applications. *arXiv preprint arXiv:2503.10362* (2025).

[11] Clemens Brunner, Robert Leeb, Gernot Müller-Putz, Alois Schlögl, and Gert Pfurtscheller. 2008. BCI Competition 2008–Graz data set A. *Institute for knowledge discovery (laboratory of brain-computer interfaces), Graz University of Technology* 16, 1–6 (2008), 34.

[12] Gyorgy Buzsaki and Andreas Draguhn. 2004. Neuronal oscillations in cortical networks. *science* 304, 5679 (2004), 1926–1929.

[13] Donghong Cai, Junru Chen, Yang Yang, Teng Liu, and Yafeng Li. 2023. Mbrain: A multi-channel self-supervised learning framework for brain signals. In *Proceedings of the 29th ACM SIGKDD Conference on Knowledge Discovery and Data Mining*. 130–141.

[14] Chi-Sheng Chen, Ying-Jung Chen, and Aidan Hung-Wen Tsai. 2025. Large Cognition Model: Towards Pretrained EEG Foundation Model. *arXiv preprint arXiv:2502.17464* (2025).

[15] Ting Chen, Simon Kornblith, Mohammad Norouzi, and Geoffrey Hinton. 2020. A simple framework for contrastive learning of visual representations. In *International conference on machine learning*. PMLR, 1597–1607.

[16] Yuqi Chen, Kan Ren, Kaitao Song, Yansen Wang, Yifan Wang, Dongsheng Li, and Lili Qiu. 2024. EEGFormer: Towards transferable and interpretable large-scale EEG foundation model. *arXiv preprint arXiv:2401.10278* (2024).

[17] Zhige Chen, Chengxuan Qin, Wenlong You, Rui Liu, Congying Chu, Rui Yang, Kay Chen Tan, and Jibin Wu. 2025. HEAR: An EEG Foundation Model with Heterogeneous Electrode Adaptive Representation. *arXiv preprint arXiv:2510.12515* (2025).

[18] Hsiang-Yun Sherry Chien, Hanlin Goh, Christopher M Sandino, and Joseph Y Cheng. 2022. Maeeg: Masked auto-encoder for eeg representation learning. *arXiv preprint arXiv:2211.02625* (2022).

[19] Wenhui Cui, Woojae Jeong, Philipp Thölke, Takfarinas Medani, Karim Jerbi, Anand A Joshi, and Richard M Leahy. 2023. Neuro-gpt: Developing a foundation model for eeg. *arXiv preprint arXiv:2311.03764* 107 (2023).

[20] Jonathan Dan, Amirhossein Shahbazzinia, Christodoulos Kechris, and David Atienza. 2025. SzCORE as a benchmark: report from the seizure detection challenge at the 2025 AI in Epilepsy and Neurological Disorders Conference. *arXiv preprint arXiv:2505.18191* (2025).

[21] Jacob Devlin, Ming-Wei Chang, Kenton Lee, and Kristina Toutanova. 2019. Bert: Pre-training of deep bidirectional transformers for language understanding. In *Proceedings of the 2019 conference of the North American chapter of the association for computational linguistics: human language technologies, volume 1 (long and short papers)*. 4171–4186.

[22] Alexandru Dimofte, Glenn Anta Bucagu, Thorir Mar Ingolfsson, Xiaying Wang, Andrea Cossettini, Luca Benini, and Yawei Li. 2025. CEREBrO: Compact Encoder for Representations of Brain Oscillations Using Efficient Alternating Attention. *arXiv preprint arXiv:2501.10885* (2025).

[23] Berkay Döner, Thorir Mar Ingolfsson, Luca Benini, and Yawei Li. 2025. Luna: Efficient and topology-agnostic foundation model for eeg signal analysis. *arXiv preprint arXiv:2510.22257* (2025).

[24] Alexey Dosovitskiy. 2020. An image is worth 16x16 words: Transformers for image recognition at scale. *arXiv preprint arXiv:2010.11929* (2020).

[25] Zitao Fang, Chenxuan Li, Hongting Zhou, Shuyang Yu, Guodong Du, Ashwqar Qasem, Yang Lu, Jing Li, Junsong Zhang, and Sim Kuan Goh. 2025. Neuript: Foundation model for neural interfaces. *arXiv preprint arXiv:2510.16548* (2025).

[26] Matteo Ferrante, Tommaso Boccato, Grigorii Rashkov, and Nicola Toschi. 2024. Towards Neural Foundation Models for Vision: Aligning EEG, MEG, and fMRI Representations for Decoding, Encoding, and Modality Conversion. *arXiv preprint arXiv:2411.09723* (2024).

[27] Luay Fraiwan and Mohanad Alkhodari. 2020. Classification of focal and non-focal epileptic patients using single channel EEG and long short-term memory learning system. *IEEE Access* 8 (2020), 77255–77262.

[28] Sam Gijssen and Kerstin Ritter. [n. d.]. EEG-Language Pretraining for Highly Label-Efficient Clinical Phenotyping. In *Forty-second International Conference on Machine Learning*.

[29] Ary L Goldberger, Luis AN Amaral, Leon Glass, Jeffrey M Hausdorff, Plamen Ch Ivanov, Roger G Mark, Joseph E Mietus, George B Moody, Chung-Kang Peng, and H Eugene Stanley. 2000. PhysioBank, PhysioToolkit, and PhysioNet: components of a new research resource for complex physiologic signals. *circulation* 101, 23 (2000), e215–e220.

[30] J. Gutttag. 2010. CHB-MIT Scalp EEG Database (version 1.0.0).

[31] Danny Dongyeop Han, Yonghyeon Gwon, Ahhyun Lucy Lee, Taeyang Lee, Seong Jin Lee, Jibin Choi, Sebin Lee, Jihyun Bang, Seungju Lee, David Keetae Park, et al. 2025. DIVER-1: Deep Integration of Vast Electrophysiological Recordings at Scale. *arXiv preprint arXiv:2512.19097* (2025).

[32] Amir Harati, Silvia Lopez, I Obeid, J Picone, MP Jacobson, and S Tobochnik. 2014. The TUH EEG CORPUS: A big data resource for automated EEG interpretation. In *2014 IEEE signal processing in medicine and biology symposium (SPMB)*. IEEE, 1–5.

[33] Kaiming He, Xinlei Chen, Saining Xie, Yanghao Li, Piotr Dollár, and Ross Girshick. 2022. Masked autoencoders are scalable vision learners. In *Proceedings of the IEEE/CVF conference on computer vision and pattern recognition*. 16000–16009.

[34] Olivier Henaff. 2020. Data-efficient image recognition with contrastive predictive coding. In *International conference on machine learning*. PMLR, 4182–4192.

[35] Jiazheng Hong, Geoffrey MacKellar, and Soheila Ghane. 2025. SAMBA: Toward a Long-Context EEG Foundation Model via Spatial Embedding and Differential Mamba. *arXiv preprint arXiv:2511.18571* (2025).

[36] James F Cavanagh jecavanagh@unm.edu. 2021. “EEG: Depression rest”. doi:10.18112/openneuro.ds003478.v1.1.0

[37] Jaehyun Jeon, Seungwoo Jeong, Yeajin Shon, and Heung-Il Suk. [n. d.]. TaKF+: A versatile and parameter-efficient tuning for EEG foundation model. ([n. d.]).

[38] Muyun Jiang, Shuailei Zhang, Zhenjie Yang, Mengjun Wu, Weibang Jiang, Zhiwei Guo, Wei Zhang, Rui Liu, Shangen Zhang, Yong Li, et al. 2025. ELASTIQ: EEG-Language Alignment with Semantic Task Instruction and Querying. *arXiv preprint arXiv:2509.24302* (2025).

[39] Wei-Bang Jiang, Yansen Wang, Bao-Liang Lu, and Dongsheng Li. 2024. NeuroLM: A Universal Multi-task Foundation Model for Bridging the Gap between Language and EEG Signals. *arXiv preprint arXiv:2409.00101* (2024).

[40] Wei-Bang Jiang, Li-Ming Zhao, and Bao-Liang Lu. 2024. Large brain model for learning generic representations with tremendous EEG data in BCI. *arXiv preprint arXiv:2405.18765* (2024).

[41] Bu Jin, Shuning Xue, Jie Jiang, Longteng Guo, Xinxin Zhu, Jin Zhou, Jing Liu, et al. [n. d.]. UniEEG: Advancing Universal EEG Representation with Electrode-Wise Time-Frequency Pretraining. ([n. d.]).

[42] Jin Jing, Wendong Ge, Shenda Hong, Marta Bento Fernandes, Zhen Lin, Chaoqi Yang, Sungtae An, Aaron F Struck, Aline Herlopian, Ioannis Karakis, et al. 2023. Development of expert-level classification of seizures and rhythmic and periodic patterns during EEG interpretation. *Neurology* 100, 17 (2023), e1750–e1762.

[43] Sangmin Jo, Jaehyun Jeon, Seungwoo Jeong, and Heung-Il Suk. 2023. Channel-aware self-supervised learning for eeg-based bci. In *2023 11th International Winter Conference on Brain-Computer Interface (BCI)*. IEEE, 1–4.

[44] Jatinder Kaur, Kulwinder Singh Parmar, and Sarbjit Singh. 2023. Autoregressive models in environmental forecasting time series: a theoretical and application review. *Environmental Science and Pollution Research* 30, 8 (2023), 19617–19641.

[45] Bob Kemp, Aeilko H Zwinderman, Bert Tuk, Hilbert AC Kamphuisen, and Josefien JL Oberye. 2000. Analysis of a sleep-dependent neuronal feedback loop: the slow-wave microcontinuity of the EEG. *IEEE Transactions on Biomedical Engineering* 47, 9 (2000), 1185–1194.

[46] Sirvan Khalighi, Teresa Sousa, José Moutinho Santos, and Urbano Nunes. 2016. ISRUC-Sleep: A comprehensive public dataset for sleep researchers. *Computer methods and programs in biomedicine* 124 (2016), 180–192.

[47] Diederik P Kingma and Max Welling. 2013. Auto-encoding variational bayes. *arXiv preprint arXiv:1312.6114* (2013).

[48] Sander Koelstra, Christian Muhl, Mohammad Soleymani, Jong-Seok Lee, Ashkan Yazdani, Tournajd Ebrahimi, Thierry Pun, Anton Nijholt, and Ioannis Patras. 2011. Deep: A database for emotion analysis; using physiological signals. *IEEE transactions on affective computing* 3, 1 (2011), 18–31.

[49] Demetres Kostas, Stephane Aroca-Ouellette, and Frank Rudzicz. 2021. BENDR: Using transformers and a contrastive self-supervised learning task to learn from massive amounts of EEG data. *Frontiers in Human Neuroscience* 15 (2021), 653659.

[50] Vamsi Kumar, Likith Reddy, Shivam Kumar Sharma, Kamalaker Dadi, Chiranjeevi Yarra, Raju S Bapi, and Srijiresh Rajendran. 2022. muIEEG: a multi-view representation learning on EEG signals. In *International Conference on Medical Image Computing and Computer-Assisted Intervention*. Springer, 398–407.

[51] Jii Kwon and Youmin Shin. 2026. Foundation Models for Neural Signal Decoding: EEG-Centered Perspectives Toward Unified Representations. *European Journal of Neuroscience* 63, 1 (2026), e70376.

[52] Cheol-Hui Lee, Hakseung Kim, Byung C Yoon, and Dong-Joo Kim. 2025. Toward Foundational Model for Sleep Analysis Using a Multimodal Hybrid Self-Supervised Learning Framework. *arXiv preprint arXiv:2502.17481* (2025).

[53] Harim Lee, Eunseon Seong, and Dong-Kyu Chae. 2022. Self-Supervised Learning with Attention-based Latent Signal Augmentation for Sleep Staging with Limited Labeled Data.. In *IJCAI*. 3868–3876.

[54] Ang Li, Zikai Wang, Liuyin Yang, Zhenyu Wang, Tianheng Xu, Honglin Hu, and Marc M Van Hulle. 2025. CoMET: A Contrastive-Masked Brain Foundation Model for Universal EEG Representation. *arXiv preprint arXiv:2509.00314* (2025).

[55] Fan Li, Rui Yan, Reza Mahini, Lai Wei, Zhiqiang Wang, Klaus Mathiak, Rong Liu, and Fengyu Cong. 2021. End-to-end sleep staging using convolutional neural network in raw single-channel EEG. *Biomedical Signal Processing and Control* 63 (2021), 102203.

[56] Hongqi Li, Yitong Chen, Yujuan Wang, Weihang Ni, and Haodong Zhang. 2025. Foundation models for cross-domain eeg analysis application: A survey. *arXiv preprint arXiv:2508.15716* (2025).

[57] Jiahui Li, Xin Chen, Fanqi Shen, Junru Chen, Yuxin Liu, Daoze Zhang, Zhizhang Yuan, Fang Zhao, Meng Li, and Yang Yang. 2025. Deep learning-powered electrical brain signals analysis: Advancing neurological diagnostics. *IEEE Reviews in Biomedical Engineering* (2025).

[58] Xiaomin Li and Vangelis Mettsis. 2022. Spp-eegnet: An input-agnostic self-supervised eeg representation model for inter-dataset transfer learning. In *International Conference on Computing and Information Technology*. Springer, 173–182.

[59] Chenyu Liu, Yiqiu Deng, Tianyu Liu, Jinan Zhou, Xinliang Zhou, Ziyu Jia, and Yi Ding. 2025. ECHO: Toward Contextual Seq2Seq Paradigms in Large EEG Models. *arXiv preprint arXiv:2509.22556* (2025).

[60] Hanwen Liu, Daniel Hajnaligol, Benny Antony, Aiguo Han, and Xuan Wang. 2024. Eeg2text: Open vocabulary eeg-to-text decoding with eeg pre-training and multi-view transformer. *arXiv preprint arXiv:2405.02165* (2024).

[61] Huan Liu, Shusen Yang, Yuzhe Zhang, Mengze Wang, Fanyu Gong, Chengxi Xie, Guanjian Liu, Zeyun Liu, Yong-Jin Liu, Bao-Liang Lu, et al. 2025. Liberer: A comprehensive benchmark and algorithm library for eeg-based emotion recognition. *IEEE Transactions on Affective Computing* (2025).

[62] Xiao Liu, Fanjin Zhang, Zhenyu Hou, Li Mian, Zhaoyu Wang, Jing Zhang, and Jie Tang. 2021. Self-supervised learning: Generative or contrastive. *IEEE transactions on knowledge and data engineering* 35, 1 (2021), 857–876.

[63] Catherine Lloyd, Loic Lorentre Lemoine, Reiyen Al-Shaikh, Kim Tien Ly, Hakan Kayan, Charith Perera, and Nhat Pham. 2024. Stress-GPT: Stress detection with an EEG-based foundation model. In *Proceedings of the 30th Annual International Conference on Mobile Computing and Networking*. 2341–2346.

[64] Sandra K Loo, Alexander Cho, T Sigi Hale, James McGough, James McCracken, and Susan L Smalley. 2013. Characterization of the theta to beta ratio in ADHD: identifying potential sources of heterogeneity. *Journal of attention disorders* 17, 5 (2013), 384–392.

[65] Fabien Lotte, Laurent Bougrain, Andrzej Cichocki, Maureen Clerc, Marco Congedo, Alain Rakotomamonjy, and Florian Yger. 2018. A review of classification algorithms for EEG-based brain–computer interfaces: a 10 year update. *Journal of neural engineering* 15, 3 (2018), 031005.

[66] Weiheng Lu, Chunfeng Song, Jiamian Wu, Pengyu Zhu, Yuchen Zhou, Weijian Mai, Qihao Zheng, and Wanli Ouyang. 2025. UniMind: Unleashing the Power of LLMs for Unified Multi-Task Brain Decoding. *arXiv preprint arXiv:2506.18962* (2025).

[67] Jingying Ma, Feng Wu, Qika Lin, Yucheng Xing, Chenyu Liu, Ziyu Jia, and Mengling Feng. 2025. CodeBrain: Bridging Decoupled Tokenizer and Multi-Scale Architecture for EEG Foundation Model. *arXiv preprint arXiv:2506.09110* (2025).

[68] Umberto Michelucci. 2022. An introduction to autoencoders. *arXiv preprint arXiv:2201.03898* (2022).

[69] Andreas Miltiadous, Katerina D. Tzimourta, Theodora Afrantou, Panagiotis Ioannidis, Nikolaos Grigoriadis, Dimitrios G. Tsalikakis, Pantelis Angelidis, Markos G. Tsipouras, Evripidis Glavas, Nikolaos Giannakeas, and Alexandros T. Tzallas. 2023. “A dataset of 88 EEG recordings from: Alzheimer’s disease, Frontotemporal dementia and Healthy subjects”. doi:doi:10.18112/openneuro.ds004504.v1.0.2

[70] Navid Mohammadi Foumani, Geoffrey Mackellar, Soheila Ghane, Saad Irtza, Nam Nguyen, and Mahsa Salehi. 2024. Eeg2rep: enhancing self-supervised EEG representation through informative masked inputs. In *Proceedings of the 30th ACM SIGKDD Conference on Knowledge Discovery and Data Mining*. 5544–5555.

[71] Mostafa Neo Mohsenvand, Mohammad Rasool Izadi, and Pattie Maes. 2020. Contrastive representation learning for electroencephalogram classification. In *Machine Learning for Health*. PMLR, 238–253.

[72] Ali Motie Nasrabadi, Armin Allahverdy, Mehdi Samavati, and Mohammad Reza Mohammadi. 2020. EEG data for ADHD / Control children. doi:10.21227/rzfh-zn36

[73] Wajid Mumtaz. 2016. MDD Patients and Healthy Controls EEG Data (New). (11 2016). doi:10.6084/m9.figshare.4244171.v2

[74] Michael Murias, James M Swanson, and Ramesh Srinivasan. 2007. Functional connectivity of frontal cortex in healthy and ADHD children reflected in EEG coherence. *Cerebral Cortex* 17, 8 (2007), 1788–1799.

[75] Petr Nejedly, Vaclav Kremen, Vladimir Sladky, Jan Cimbalnik, Petr Klimes, Filip Plesinger, Filip Mivalt, Vojtech Travnick, Ivo Viscor, Martin Pail, et al. 2020. Multicenter intracranial EEG dataset for classification of graphoelements and artifactual signals. *Scientific data* 7, 1 (2020), 179.

[76] Jennifer J Newson and Tara C Thiagarajan. 2019. EEG frequency bands in psychiatric disorders: a review of resting state studies. *Frontiers in human neuroscience* 12 (2019), 521.

[77] Iyad Obeid and Joseph Picone. 2016. The temple university hospital EEG data corpus. *Frontiers in neuroscience* 10 (2016), 196.

[78] Mattson Ogg and William G Coon. 2024. Self-supervised transformer model training for a sleep-eeg foundation model. In *2024 46th Annual International Conference of the IEEE Engineering in Medicine and Biology Society (EMBC)*. IEEE, 1–6.

[79] B Orkan Olcay and Bilge Karaçalı. 2023. Time-resolved EEG signal analysis for motor imagery activity recognition. *Biomedical Signal Processing and Control* 86 (2023), 105179.

[80] Aaron van den Oord, Yazhe Li, and Oriol Vinyals. 2018. Representation learning with contrastive predictive coding. *arXiv preprint arXiv:1807.03748* (2018).

[81] Yassine El Ouahidi, Jonathan Lys, Philipp Thölke, Nicolas Farrugia, Bastien Pasdeloup, Vincent Gripon, Karim Jerbi, and Giulia Lioi. 2025. REVE: A Foundation Model for EEG–Adapting to Any Setup with Large-Scale Pretraining on 25,000 Subjects. *arXiv preprint arXiv:2510.21585* (2025).

[82] Alec Radford, Jeffrey Wu, Rewon Child, David Luan, Dario Amodei, Ilya Sutskever, et al. 2019. Language models are unsupervised multitask learners. *OpenAI blog* 1, 8 (2019), 9.

[83] Abdellah Rahmani, Arun Venkitaraman, and Pascal Frossard. 2023. A Meta-GNN approach to personalized seizure detection and classification. In *ICASSP 2023–2023 IEEE International Conference on Acoustics, Speech and Signal Processing (ICASSP)*. IEEE, 1–5.

[84] Alexander P. Rockhill, Nicko Jackson, Jobi George, Adam Aron, and Nicole C. Swann. 2021. “UC San Diego Resting State EEG Data from Patients with Parkinson’s Disease”. doi:doi:10.18112/openneuro.ds002778.v1.0.5

[85] Ayan Seal, Rishabh Bajpai, Jagriti Agnihotri, Anis Yazidi, Enrique Herrera-Viedma, and Ondrej Krejcar. 2021. DeprNet: A deep convolution neural network framework for detecting depression using EEG. *IEEE Transactions on Instrumentation and Measurement* 70 (2021), 1–13.

[86] Ali Shoeb. 2009. *Application of Machine Learning to Epileptic Seizure Onset Detection and Treatment*. Ph.D. Dissertation. Massachusetts Institute of Technology.

[87] Rahul Thapa, Bryan He, Magnus Ruud Kjaer, H Moore IV, Gauri Ganjoo, Emmanuel Mignot, and James Zou. 2024. Sleepfm: foundation model for sleep analysis. In *ICLR Workshop on Learning from Time Series For Health*.

[88] Aaron Van Den Oord, Oriol Vinyals, et al. 2017. Neural discrete representation learning. *Advances in neural information processing systems* 30 (2017).

[89] Neeraj Wagh, Jionghao Wei, Samarth Rawal, Brent Berry, Leland Barnard, Benjamin Brinkmann, Gregory Worrell, David Jones, and Yogatheeswar Varatharajah. 2021. Domain-guided self-supervision of EEG data improves downstream classification performance and generalizability. In *Machine Learning for Health*. PMLR, 130–142.

[90] Christopher Wang, Vighnesh Subramaniam, Adam Uri Yaari, Gabriel Kreiman, Boris Katz, Ignacio Cases, and Andrei Barbu. 2023. BrainBERT: Self-supervised representation learning for intracranial recordings. *arXiv preprint arXiv:2302.14367* (2023).

[91] Guangyu Wang, Wenchao Liu, Yuhong He, Cong Xu, Lin Ma, and Haifeng Li. 2024. Eegpt: Pretrained transformer for universal and reliable representation of eeg signals. *Advances in Neural Information Processing Systems* 37 (2024), 39249–39280.

[92] Jiquan Wang, Sha Zhao, Zhiling Luo, Yangxuan Zhou, Haiteng Jiang, Shijian Li, Tao Li, and Gang Pan. 2024. CBraMod: A Criss-Cross Brain Foundation Model for EEG Decoding. *arXiv preprint arXiv:2412.07236* (2024).

[93] Limin Wang, Toyotaro Suzumura, and Hiroki Kanezashi. 2024. Graph-Enhanced EEG Foundation Model. *arXiv preprint arXiv:2411.19507* (2024).

[94] Yihe Wang, Nan Huang, Nadia Mammone, Marco Cecchi, and Xiang Zhang. 2025. LEAD: Large Foundation Model for EEG-Based Alzheimer’s Disease Detection. *arXiv preprint arXiv:2502.01678* (2025).

[95] Xinxiu Wei, Kanhao Zhao, Yong Jiao, Nancy B Carlisle, Hua Xie, Gregory A Fonzo, and Yu Zhang. 2025. Multi-modal cross-domain self-supervised pre-training for fMRI and EEG fusion. *Neural Networks* 184 (2025), 107066.

[96] Xinxiu Wei, Kanhao Zhao, Yong Jiao, Nancy B Carlisle, Hua Xie, and Yu Zhang. 2024. Pre-Training Graph Contrastive Masked Autoencoders are Strong Distillers for EEG. *arXiv preprint arXiv:2411.19230* (2024).

[97] Weining Weng, Yang Gu, Shuai Guo, Yuan Ma, Zhaohua Yang, Yuchen Liu, and Yiqiang Chen. 2025. Self-supervised learning for electroencephalogram: A systematic survey. *Comput. Surveys* 57, 12 (2025), 1–38.

[98] Anqi Wu, Yifan Zhang, Yang Yu, and Ling-Li Zeng. 2024. EEG-ARNet: An Autoregressive Pre-training Model for Extracting EEG Features. In *2024 5th*

International Conference on Computers and Artificial Intelligence Technology (CAIT). IEEE, 255–259.

[99] Di Wu, Siyuan Li, Jie Yang, and Mohamad Sawan. 2022. neuro2vec: Masked fourier spectrum prediction for neurophysiological representation learning. *arXiv preprint arXiv:2204.12440* (2022).

[100] Di Wu, Siyuan Li, Jie Yang, and Mohamad Sawan. 2024. Neuro-BERT: Rethinking Masked Autoencoding for Self-Supervised Neurological Pretraining. *IEEE Journal of Biomedical and Health Informatics* (2024).

[101] Jiamin Wu, Zichen Ren, Junyu Wang, Pengyu Zhu, Yonghao Song, Mianxin Liu, Qihao Zheng, Lei Bai, Wanli Ouyang, and Chunfeng Song. 2025. AdaBrain-bench: Benchmarking brain foundation models for brain-computer interface applications. *arXiv preprint arXiv:2507.09882* (2025).

[102] Chuqin Xiang, Xinrui Fan, Duo Bai, Ke Lv, and Xu Lei. 2024. “A Resting-state EEG Dataset for Sleep Deprivation”. doi:doi:10.18112/openneuro.ds004902.v1.0.5

[103] Qinfan Xiao, Ziyun Cui, Chi Zhang, Siqi Chen, Wen Wu, Andrew Thwaites, Alexandra Woolgar, Bowen Zhou, and Chao Zhang. 2025. BrainOmni: A Brain Foundation Model for Unified EEG and MEG Signals. *arXiv preprint arXiv:2505.18185* (2025).

[104] Wei Xiong, Jiangtong Li, Jie Li, and Kun Zhu. 2025. Eeg-fm-bench: A comprehensive benchmark for the systematic evaluation of eeg foundation models. *arXiv preprint arXiv:2508.17742* (2025).

[105] Chaoqi Yang, M Westover, and Jimeng Sun. 2023. Biot: Biosignal transformer for cross-data learning in the wild. *Advances in Neural Information Processing Systems* 36 (2023), 78240–78260.

[106] Wenchao Yang, Weidong Yan, Wenkang Liu, Yulan Ma, and Yang Li. 2025. THD-BAR: Topology Hierarchical Derived Brain Autoregressive Modeling for EEG Generic Representations. *arXiv preprint arXiv:2511.13733* (2025).

[107] Zhizhang Yuan, Fanqi Shen, Meng Li, Yuguo Yu, Chenhao Tan, and Yang Yang. 2024. BrainWave: A Brain Signal Foundation Model for Clinical Applications. *arXiv preprint arXiv:2402.10251* (2024).

[108] Tongfai Yue, Shuning Xue, Xuange Gao, Yeping Tang, Longteng Guo, Jie Jiang, and Jing Liu. 2024. EEGPT: Unleashing the Potential of EEG Generalist Foundation Model by Autoregressive Pre-training. *arXiv preprint arXiv:2410.19779* (2024).

[109] Ziyi Zeng, Zhenyang Cai, Yixi Cai, Xidong Wang, Junying Chen, Rongsheng Wang, Yipeng Liu, Siqi Cai, Benyou Wang, Zhiguo Zhang, et al. 2025. Wavemind: Towards a conversational eeg foundation model aligned to textual and visual modalities. *arXiv preprint arXiv:2510.00032* (2025).

[110] George Zerveas, Srideepika Jayaraman, Dhaval Patel, Anuradha Bhamidipaty, and Carsten Eickhoff. 2021. A transformer-based framework for multivariate time series representation learning. In *Proceedings of the 27th ACM SIGKDD conference on knowledge discovery & data mining*, 2114–2124.

[111] Daoze Zhang, Zhizhang Yuan, Junru Chen, Kerui Chen, and Yang Yang. 2024. Brant-X: A Unified Physiological Signal Alignment Framework. In *Proceedings of the 30th ACM SIGKDD Conference on Knowledge Discovery and Data Mining*, 4155–4166.

[112] Daoze Zhang, Zhizhang Yuan, Yang Yang, Junru Chen, Jingjing Wang, and Yafeng Li. 2023. Brant: Foundation model for intracranial neural signal. *Advances in Neural Information Processing Systems* 36 (2023), 26304–26321.

[113] Wenrui Zhang, Ling Yang, Shijia Geng, and Shenda Hong. 2023. Self-supervised time series representation learning via cross reconstruction transformer. *IEEE Transactions on Neural Networks and Learning Systems* (2023).

[114] Xiang Zhang, Lina Yao, Xianzhi Wang, Jessica Monaghan, David McAlpine, and Yu Zhang. 2021. A survey on deep learning-based non-invasive brain signals: recent advances and new frontiers. *Journal of neural engineering* 18, 3 (2021), 031002.

[115] Xiang Zhang, Ziyuan Zhao, Theodoros Tsiligkaridis, and Marinika Zitnik. 2022. Self-supervised contrastive pre-training for time series via time-frequency consistency. *Advances in neural information processing systems* 35 (2022), 3988–4003.

[116] Zihan Zhang, Xiao Ding, Yu Bao, Yi Zhao, Xia Liang, Bing Qin, and Ting Liu. 2024. Chisco: An EEG-based BCI dataset for decoding of imagined speech. *Scientific Data* 11, 1 (2024), 1265.

[117] Wei-Long Zheng, Wei Liu, Yifei Lu, Bao-Liang Lu, and Andrzej Cichocki. 2018. Emotionmeter: A multimodal framework for recognizing human emotions. *IEEE transactions on cybernetics* 49, 3 (2018), 1110–1122.

[118] Wei-Long Zheng and Bao-Liang Lu. 2015. Investigating critical frequency bands and channels for EEG-based emotion recognition with deep neural networks. *IEEE Transactions on autonomous mental development* 7, 3 (2015), 162–175.

[119] Jinzhao Zhou, Zehong Cao, Yiqun Duan, Connor Barkley, Daniel Leong, Xiaowei Jiang, Quoc-Toan Nguyen, Ziyi Zhao, Thomas Do, Yu-Cheng Chang, et al. 2025. Pretraining Large Brain Language Model for Active BCI: Silent Speech. *arXiv preprint arXiv:2504.21214* (2025).

[120] Xinliang Zhou, Chenyu Liu, Zhiheng Chen, Kun Wang, Yi Ding, Ziyu Jia, and Qingsong Wen. 2025. Brain foundation models: A survey on advancements in neural signal processing and brain discovery. *arXiv preprint arXiv:2503.00580* (2025).

[121] Yangxuan Zhou, Sha Zhao, Jiquan Wang, Haiteng Jiang, Shijian Li, Tao Li, and Gang Pan. [n. d.]. BrainUICL: An unsupervised individual continual learning framework for EEG applications. In *The Thirteenth International Conference on Learning Representations*.

[122] Qiuishi Zhu, Xiaoying Zhao, Jie Zhang, Yu Gu, Chao Weng, and Yuchen Hu. 2023. EEG2VEC: Self-supervised electroencephalographic representation learning. *arXiv preprint arXiv:2305.13957* (2023).

[123] Igor Zyma, Sergii Tukaev, Ivan Seleznov, Ken Kiyono, Anton Popov, Mariia Chernykh, and Oleksii Shpenkov. 2019. Electroencephalograms during mental arithmetic task performance. *Data* 4, 1 (2019), 14.

A SSL Paradigm

A.1 Contrastive-based Method

A.1.1 Augmentation contrast. Augmentation-based contrastive learning constructs positive pairs by applying transformation operators a_s to the same input signal, with representation learning driven by enforcing invariance across augmented views. Early BFM works primarily focused on expanding the effective view space induced by a_s . SeqCLR [71] adapts SimCLR [15] to multichannel EEG by recombining channels to expand the augmentation-induced view space and enforce consistency across views. SppEEGNet [58] further applies a suite of EEG-specific augmentations and forms positive pairs within sliding windows on a 2D signal representation, which helps reduce cross-dataset sampling-rate mismatch. BIOT [105] introduces channel-level augmentations tailored to biosignals. Nevertheless, contrastive objectives can suffer from false negatives, especially in sleep staging, where adjacent segments may share labels. SSLAPP [53] addresses this by adversarially generating high-quality positives and performing attention-guided augmentation in latent space, mitigating semantic collisions in pair construction.

As view construction strategies matured, research attention gradually shifted toward the design of the encoder $\mathcal{F}(\cdot)$ to better capture EEG dynamics. Early approaches predominantly relied on CNN-based architectures [50, 58, 71], which primarily model local temporal patterns. Recognizing the intrinsically non-stationary and multi-scale nature of neural signals, later works incorporate temporal-spectral duality into representation learning. TF-C [115] enforces consistency between time-domain and frequency-domain embeddings of the same signal, explicitly coupling complementary signal views. More recently, transformer-based encoders have been introduced to support cross-dataset and cross-subject learning at scale. BIOT [105] employs a biosignal transformer to unify heterogeneous modalities, while LEAD [95] further regularizes representations through subject-level consistency, encouraging invariant embeddings across samples from the same individual.

A.1.2 Contrastive Predictive Coding. Inspired by BERT and wav2vec 2.0[6], Bendlr[49] encodes EEG segments into a unified sequence of learned vector representations. Maeeg[18] and GEFM[93] have similar architecture to Bendlr with different PT mindset. Although Bendlr can extract features well, it ignores spatial information. To address this issue, several models have been proposed. GEFM adds a graph structure to Bendlr and proposes a sequence length adjustment mechanism before GNN to make EEG signal lengths consistent for fixed-length node features in GNN. Zhu et al. [122] incorporated spatial information through channel-mixing augmentation, effectively enhancing dataset diversity and improving the performance of the contrastive EEG2Vec framework. Another line of work extends CPC to better exploit multichannel structure and continual

data streams. MBrain [13] augments CPC with spatial awareness by aggregating multichannel semantics to predict single-channel local representations, encouraging implicit spatio-temporal dependencies across channels. BrainUICL [121] further combines CPC with replay-based continual learning, and the contrastive model is incrementally updated via joint training with replayed samples.

A.1.3 Cross-modal Contrast. Inspired by multimodal contrastive learning, BFM_s extend cross-modal alignment to EEG, where “modality” arises from the inherent heterogeneity of brain recordings. At the intra-signal level, different views of the same EEG (e.g., raw waveforms vs. time-frequency representations) can serve as distinct modalities. MuLEEG [50] follows this paradigm by contrasting multi-view raw signals with spectrograms. Beyond view-level heterogeneity, MCSP [95] mines complementary information across modalities and models latent interactions within each domain, particularly spatial structure via graphs. For truly multi-sensor settings, SleepFM [87] jointly embeds three biosignal modalities using both pairwise contrast and a leave-one-out objective, aligning each modality to the average of the others. Brant-X [111] further targets EEG-EXG coupling by aligning representations at both patch and sequence levels, capturing correlations at fine- and coarse-grained semantic scales. Moving to heterogeneous cross-modal alignment beyond biosignals, Ferrante et al. [26] align neural recordings with visual stimuli, demonstrating that visual content can be decoded from neural data and that images can be mapped into neural representation spaces.

A.2 Generative-based Methods

A.2.1 Autoregressive. The success of autoregressive (AR) language models in modeling long-range dependencies via next-token prediction has motivated the adoption in BFM_s. Using a decoder-only transformer architecture, GPT-style models [82] have been adapted to EEG pretraining in several BFM_s [19, 63, 91, 108]. Early efforts such as Neuro-GPT [19] segment continuous EEG into fixed-length chunks and treat each chunk as a token, enabling a GPT model $\mathcal{G}_{\theta_2}(\cdot)$ to learn spatio-temporal structure by predicting masked segments. Building on this framework, Stress-GPT [63] fine-tunes the pretrained model for stress-related tasks, demonstrating the transferability of AR-pretrained representations.

Subsequent works refine the tokenization and prediction strategy to better reflect EEG-specific structure. EEGPT-2 [108] adopts an electrode-wise autoregressive formulation, treating each electrode signal x_i^e as a basic token and modeling temporal dependencies through an Electrode Temporal Encoder. EEG2Rep [70] shifts target prediction into latent space via context-driven masking and introduces a semantic subsequence preserving mechanism to provide more informative masked inputs. Inspired by large language models, NeuroLM [39] generalizes autoregressive pretraining to multi-channel EEG, explicitly modeling inter-channel dependencies. More recently, LBLM [119] unifies temporal and spectral autoregression to capture spectro-temporal dynamics, while ECHO [59] constructs discrete, prompt-like context supports encoding hierarchical signal-task-label relations, improving in-context learning for downstream EEG tasks.

A.2.2 Autoencoder. Autoencoder is the most common method in BFM_s pretraining. To learn informative representations $\mathcal{M}(x)$, AE-based BFM_s rely on carefully designed disturbance mechanisms that force reconstruction from partial observations. Masked Autoencoders (MAE) [33] randomly mask input regions and reconstruct missing content from visible context, encouraging the model to capture global structure. Inspired by both BENDR [49] and MAE, MAEEG [18] and GEFM [93] adopt masked reconstruction for EEG pretraining. UniEEG [41] further introduces Masked Signal Modeling (MSM) with electrode-wise masking, while EEGPT-1 [91] embeds local spatio-temporal patches as tokens and proposes a dual SSL objective combining mask-based reconstruction with spatio-temporal alignment.

Beyond masking strategies, modern AE-based BFM_s primarily differ in the design of the encoder $\mathcal{F}_{\theta_1}(\cdot)$, which must model long-range temporal dependencies while capturing cross-channel interactions. Early models such as BrainBERT [90] largely encode electrodes independently, limiting spatial coupling. Subsequent works introduce stronger spatial inductive biases: EEG2TEXT [60] employs multi-view attention to reflect region-wise processing, while CBraMod [92] adopts a criss-cross encoder that alternates spatial-temporal attention with asymmetric conditional positional encoding. To handle heterogeneous montages, LUNA [23] unifies variable electrode layouts into a fixed latent space via learned queries, and REVE [81] injects anatomical priors through 4D positional embeddings derived from electrode coordinates and time indices. Beyond attention-based designs, Mamba-style encoders enable linear-time sequence modeling for long recordings. Synth-SleepNet [52] introduces a Mamba-based Temporal Context Module for inter-epoch dependencies, while SAMBA [35] proposes a Multi-head Differential Mamba to suppress background noise while aggregating contextual information.

However, the inherent randomness, non-stationarity, and non-linearity of neurophysiological signals make direct amplitude reconstruction in the spatiotemporal domain suboptimal [99]. As a result, recent BFM_s increasingly perform masking and reconstruction in transformed spaces $\mathcal{T}_d(\cdot)$ or low-dimensional latent variables z_i . Neuro2vec [99] pioneers denoising in the Fourier domain, while CRT [113] performs cross-domain dropping-reconstruction to align time- and frequency-domain representations. Building on Fourier-domain MAE, Neuro-BERT [100] introduces Fourier Inversion Prediction (FIP) as a pretraining objective. In parallel, spectrogram-based reconstruction has gained traction due to its rich time-frequency semantics, supporting both signal understanding and downstream learning [78, 90, 107].

Most AE-based BFM_s are developed for non-invasive EEG, while intracranial EEG (IEEG) remains comparatively underexplored. To bridge this gap, BrainBERT [90], Brant [112], and Brainwave [107] extend AE-based pretraining to SEEG recordings. BrainBERT leverages SEEG data from subjects watching videos, Brant adopts a dual-encoder MAE to jointly capture temporal dependencies and spatial correlations, and Brainwave scales pretraining to over 16,000 subjects, setting new benchmarks for diagnosis tasks. While these approaches substantially improve performance, they often increase model size. To address this, CEReBrO [22] proposes a compact

encoder that represents brain oscillations through alternating attention, offering a parameter-efficient alternative for AE-based BFM.

A.2.3 Codebook. The codebook mechanism, originally introduced by Vector-Quantized Variational Autoencoders (VQ-VAE) [88], offers a key advantage over standard VAEs by discretizing continuous representations into a finite set of tokens. Recently, this paradigm has been adapted to EEG and iEEG modeling, where encoder outputs are quantized into discrete codebook entries via a quantization operator $Q * \theta_3(\cdot)$ prior to decoding. Such discretization enables token-based representations of neural signals, bridging continuous biosignals with sequence modeling frameworks. The codebook is optimized using the vector-quantization objective: $\mathcal{L}_{vq} = ||sg[Q_{\theta_3}(z_i)] - z_i||_2^2 + \beta ||sg[z_i] - Q_{\theta_3}(z_i)||_2^2$ where $sg[\cdot]$ denotes the stop-gradient operator. Compared to conventional masked reconstruction, vector-quantized transformers often learn more generalizable neural representations and exhibit strong adaptability across heterogeneous downstream tasks.

A central challenge of this paradigm lies in learning an effective quantization operator $Q_{\theta_3}(\cdot)$. EEGFormer [16] first applies codebook-based discretization to EEG pretraining, generating discrete indices that yield transferable and interpretable representations. LaBraM [40] further introduces a neural codebook that quantizes patch-level embeddings, with the codebook optimized through reconstruction in the Fourier domain. BioSerenity-E1 [10] adopts a transformer-based VQ-VAE to tokenize EEG spectra and performs masked token prediction, forcing the model to capture complex spatiotemporal dependencies and achieving state-of-the-art diagnostic performance. Beyond reconstruction-based objectives, NeuroLM [39] extends this line of work by introducing vector-quantized time-frequency prediction and aligning EEG tokens with textual representations via adversarial training. After discretization, it employs multi-channel autoregressive modeling, enabling LLMs to predict EEG tokens in a manner analogous to language modeling.

While codebook learning is often instantiated within autoencoder-style frameworks, it should be viewed as a general representation mechanism rather than a method specific to AE-based BFM. Discrete neural tokens can serve as a unifying interface across reconstruction, contrastive, and autoregressive paradigms, motivating their independent treatment in this appendix.

A.3 Other Advanced Method

A.3.1 explicit predictive. In the context of EEG, several predictive tasks have been specifically proposed by updating the form of $\mathcal{G}_{\theta_2}(\cdot)$ to better align with neurophysiological characteristics. Domain-guided CL [89] introduces Behavioral State Estimation, which predicts the delta-beta ratio to capture arousal-related spectral patterns. The Stopped Band Prediction pretext task[43] focuses on learning frequency-aware representations by asking the model to identify which frequency band has been suppressed in the input signal to capture frequency information. And the Temporal Trend Identification task[43] aims to extract temporal dynamics by classifying pre-defined trends. Although these tasks are neurophysiologically interpretable, their dependence on specific assumptions about signal behavior has still limited their adoption in BFM.

A.3.2 Hybrid-based. Hybrid SSL combines multiple self-supervised objectives within a unified framework to exploit complementary learning signals [97]. In EEG, Domain-guided contrastive learning [89] designs SSL pretext tasks grounded in neurophysiological priors, leveraging similarity of brain activity as well as behavioral-state and age-related differences. EEG-DisGCMAE [96] further introduces a graph-structured hybrid that couples Graph Contrastive pretraining with Graph MAE. LCM [14] follows a different route, using masked generative reconstruction as the primary objective and adding a momentum-updated target encoder with a contrastive term to stabilize representation learning. More broadly, BFM increasingly pair contrastive objectives with generative modeling to jointly enforce cross-view consistency and preserve signal structure [14, 52, 54, 91]. Other hybrids integrate reconstruction with autoregressive prediction to capture both local structure and long-range temporal dynamics [38, 106], and may further incorporate adversarial objectives for domain-aware alignment [39, 53].

A.3.3 Instruction-tuned. Recent instruction-tuned BFM bridge EEG representations with language semantics through lightweight alignment modules while keeping LLM backbones mostly frozen. NeuroLM[39] discretizes EEG into temporal-frequency tokens via VQ encoding and aligns EEG and text embeddings through domain-adversarial learning, followed by multi-channel autoregressive pre-training and prompt-based multi-task instruction tuning. TaKF+[37] emphasizes parameter-efficient transfer by injecting task information through adapters and cross-attention blocks after masked patch pretraining. UniMind[66] proposes a Neuro-Language Connector that extracts task-relevant temporal-spatial semantics using learnable queries with task-aware routing, and aligns them to the LLM latent space for instruction-conditioned generation. WaveMind[109] combines contrastive multimodal alignment with CLIP and instruction tuning on a large EEG instruction dataset, enabling conversational EEG understanding across tasks.

B Dataset

This section summarizes additional dataset characteristics omitted from the main text for brevity (Table 7). These attributes reflect dataset acquisition protocols and are provided to facilitate reproducibility and practical reuse of the benchmark. All datasets are processed under consistent cross-subject and cross-validation protocols. Dataset-specific preprocessing procedures are implemented in our open-source code. For transparency and reproducibility, the complete preprocessing pipelines for each dataset are documented in the `data_preprocess` directory. All datasets used Brain4FMs are publicly released; ethics and fairness considerations are therefore limited, as no new data collection is involved.

To further support transparent benchmarking, pretraining data sources of the evaluated BFM are documented whenever disclosed by the original papers or released checkpoints. In selecting downstream benchmarks, overlap with commonly used pretraining corpora was minimized a priori: most downstream datasets are disjoint from the dominant pretraining sources (e.g., TUH [77]/TUEG [32] or large private collections). Potential overlap is therefore limited to a small subset of models that incorporate BCI-oriented resources during pretraining (e.g., the SEED series and BCI Competition IV, overlapping with SEED-IV and BCI-2a). In addition, some

models leverage task-related corpora for AD, SD, or sleep staging pretraining. The downstream datasets were curated to avoid direct dataset-level reuse in these categories whenever possible. Brain4FMs evaluates models as released under unified protocols rather than re-pretraining leave-dataset-out variants. Empirically, performance differences cannot be explained by partial overlap alone under the standardized cross-subject fine-tuning setting, suggesting that pretraining scale, data diversity, SSL objectives, and architectural choices also contribute.

Table 7: Public EEG/iEEG datasets used in the benchmark, listing the number of channels (#Ch), sequence length (SeqLen), sampling frequency, total recording duration, and dataset category.

Name	#Ch	SeqLen	Frequency	Total Time	Category
CHBMIT [30]	23	10s	256	686 h	2
MAYO [75]	1	3s	5000 → 1000	94.38 h	2
FNUSA [75]	1	3s	5000 → 1000	149.69 h	2
Dep-BDI [36]	64	10s	500 → 250	31.5 h	2
Dep-STAI [36]	64	10s	500 → 250	31.5 h	3
MDD-64 [73]	19	10s	256	20.53 h	2
SD-28 [102]	19	5s	250	958 min	2
UCSD-ON [84]	32	10s	512 → 256	220 min	2
UCSD-OFF [84]	32	10s	512 → 256	220 min	2
ADFD [69]	19	10s	500 → 250	1164 min	2
ADHD_Adult [7]	2	5s	256	423 min	2
ADHD_Child [72]	19	5s	128	274.5 min	2
ISRUC-G1 [46]	6	30s	200	744.5 h	5
SleepEDF [45]	1	30s	100	378.7 h	5
DEAP [48]	32	10s	128	2133 min	4
SEED-IV [117]	62	4s	200	54 h	4
EEGMat [123]	32	10s	500 → 250	144 min	2
EEGMMIDB-R [29]	64	4s	160	2834 min	4
EEGMMIDB-I [29]	64	4s	160	2834 min	4
BCI-2a [11]	22	3s	250	130 min	4
Chisco-R [116]	125	3.3s	500	58.6 h	39
Chisco-I [116]	125	3.3s	500	58.6 h	39

C Experimental Setup

We evaluate all models under a unified cross-subject protocol with cross-validation, following standard practice in benchmarks. Models are finetuned for up to 50 epochs with early stopping (patience = 5) based on validation performance. For optimization, we primarily use Adam or AdamW. For a small number of BFMs, we retain their original optimizers as specified by the authors to avoid unintended performance degradation caused by altering model specific training designs. Batch sizes are adjusted according to model capacity and GPU memory constraints. To ensure comparability and avoid excessive tuning, we use fixed learning rates across all models: 1×10^{-5} for the BFMs backbone and 1×10^{-4} for the classifier head.

D Benchmark Result

We report the complete evaluation results of all 15 BFMs across 22 downstream classification tasks. For NeuroGPT, we report both encoder-only (NeuroGPT-E) and encoder-decoder (NeuroGPT-D) variants, complementing the analysis in Section 3.3.2. Full results provide comprehensive evidence for the observed cross-task performance trends among different BFMs. For binary tasks, we report

AUROC, Accuracy, F1, and F2 to capture threshold-free discrimination and positive-class detection under imbalance. For multi-class tasks, we report Accuracy, AUROC (one-vs-rest; OvR), macro-F1 (MF1), and Cohen’s κ (Kappa) to measure overall discrimination, class-wise performance, and agreement beyond chance. We report results as mean \pm standard deviation over n-fold cross-validation, and bold indicates the best performance based on unrounded values. All metrics use two decimal places, except Cohen’s κ , which uses three decimals due to its small magnitude on some datasets. In Tables 8 to 29, models are grouped by SSL paradigm and sorted by the primary metric within each group.

Table 8: Performance of BFMs on the CHBMIT dataset.

Type	Model	AUROC	Acc	F1	F2
C	MBrain	.71±.03	.73±.06	.31±.15	.28±.20
	BIOT	.56±.08	.29±.05	.41±.03	.61±.02
	Bendr	.55±.03	.59±.03	.32±.02	.36±.04
	SppEEGNet	.43±.05	.60±.06	.31±.04	.33±.05
G	BrainWave	.90±.03	.80±.12	.71±.09	.78±.04
	REVE	.84±.10	.78±.12	.63±.14	.66±.13
	NeuroGPT-E	.78±.12	.75±.07	.51±.22	.63±.16
	BrainBERT	.78±.06	.75±.10	.58±.08	.61±.09
	LaBraM	.75±.10	.73±.10	.53±.14	.57±.17
	BrainOmni	.74±.13	.67±.19	.51±.12	.56±.12
	BFM	.74±.05	.72±.03	.51±.09	.51±.14
	CBraMod	.69±.04	.70±.08	.46±.08	.49±.14
	NeuroGPT-D	.61±.07	.73±.03	.18±.23	.19±.25
	Brant	.55±.05	.70±.01	.00±.00	.00±.00
O	EEGPT	.71±.09	.67±.11	.46±.06	.51±.15
	NeuroLM	.67±.06	.54±.20	.27±.23	.38±.34

Table 9: Performance of BFMs on the MAYO dataset.

Type	Model	AUROC	Acc	F1	F2
C	Bendr	.93±.03	.90±.02	.69±.13	.75±.11
	MBrain	.92±.04	.92±.02	.70±.11	.73±.09
	BIOT	.90±.07	.88±.05	.63±.14	.72±.13
	SppEEGNet	.56±.03	.75±.05	.34±.09	.39±.09
G	BrainWave	.98±.01	.93±.02	.81±.09	.86±.03
	BrainBERT	.97±.01	.95±.01	.81±.07	.83±.07
	LaBraM	.96±.02	.93±.02	.76±.12	.80±.09
	NeuroGPT-E	.96±.02	.93±.02	.71±.07	.67±.08
	REVE	.92±.04	.89±.04	.66±.13	.72±.11
	Brant	.92±.03	.82±.12	.58±.19	.69±.14
	BrainOmni	.91±.06	.91±.02	.67±.13	.69±.12
	CBraMod	.89±.04	.87±.02	.59±.12	.64±.10
	BFM	.81±.08	.68±.08	.43±.15	.59±.14
	NeuroGPT-D	.77±.15	.88±.03	.23±.26	.19±.21
O	EEGPT	.92±.03	.90±.03	.67±.10	.70±.07
	NeuroLM	.64±.09	.72±.16	.30±.20	.37±.26

Table 10: Performance of BFM s on the FNUSA dataset.

Type	Model	AUROC	Acc	F1	F2
C	MBrain	.91±.08	.87±.08	.75±.13	.76±.16
	Bendr	.88±.06	.84±.06	.73±.11	.77±.10
	BIOT	.87±.07	.83±.08	.73±.14	.77±.10
	SppEEGNet	.64±.08	.67±.05	.48±.13	.52±.18
G	BrainWave	.92±.05	.89±.06	.83±.06	.83±.04
	NeuroGPT-E	.90±.06	.86±.05	.74±.04	.72±.11
	BrainBERT	.90±.04	.89±.04	.77±.09	.79±.08
	LaBraM	.89±.08	.82±.10	.72±.15	.76±.11
	BrainOmni	.88±.07	.84±.05	.73±.08	.75±.09
	REVE	.87±.08	.82±.07	.71±.10	.74±.08
	Brant	.87±.12	.84±.07	.75±.06	.79±.08
	BFM	.78±.12	.69±.11	.62±.05	.69±.08
	NeuroGPT-D	.72±.12	.77±.12	.30±.38	.27±.35
	CBraMod	.71±.13	.78±.08	.62±.13	.64±.12
O	EEGPT	.90±.04	.84±.06	.75±.11	.78±.08
	NeuroLM	.64±.14	.72±.17	.37±.28	.38±.35

Table 11: Performance of BFM s on the ADFD dataset.

Type	Model	AUROC	Acc	F1	F2
C	BIOT	.56±.17	.49±.12	.58±.14	.70±.24
	MBrain	.53±.12	.50±.10	.53±.12	.52±.14
	Bendr	.52±.02	.52±.01	.54±.05	.52±.07
	SppEEGNet	.52±.02	.51±.02	.51±.05	.49±.07
G	REVE	.84±.07	.77±.08	.79±.07	.79±.09
	BrainOmni	.80±.07	.71±.04	.73±.05	.72±.09
	BrainWave	.74±.05	.68±.05	.68±.10	.73±.10
	LaBraM	.72±.07	.68±.05	.68±.09	.72±.07
	BrainBERT	.59±.05	.58±.05	.60±.11	.64±.15
	BFM	.59±.08	.58±.09	.59±.12	.61±.09
	CBraMod	.55±.06	.59±.04	.41±.20	.37±.20
	NeuroGPT-E	.51±.03	.55±.01	.71±.01	.85±.01
	Brant	.50±.07	.54±.04	.70±.03	.84±.04
	NeuroGPT-D	.50±.03	.55±.01	.71±.01	.86±.01
O	EEGPT	.81±.05	.72±.05	.73±.05	.70±.07
	NeuroLM	.51±.04	.53±.03	.63±.09	.71±.16

Table 12: Performance of BFM s on the ADHD-Adult dataset.

Type	Model	AUROC	Acc	F1	F2
C	BIOT	.96±.02	.90±.04	.89±.04	.90±.05
	MBrain	.95±.03	.92±.04	.91±.04	.91±.06
	Bendr	.62±.03	.61±.04	.60±.05	.61±.06
	SppEEGNet	.51±.04	.54±.06	.36±.30	.36±.35
G	BrainOmni	.96±.02	.91±.02	.90±.03	.89±.04
	BrainWave	.96±.03	.91±.04	.91±.04	.91±.05
	REVE	.96±.02	.91±.02	.91±.02	.90±.05
	Brant	.95±.03	.89±.04	.89±.04	.90±.05
	LaBraM	.95±.04	.91±.04	.92±.04	.91±.04
	CBraMod	.95±.02	.92±.04	.91±.04	.91±.07
	NeuroGPT-E	.91±.05	.84±.06	.83±.05	.82±.03
	BFM	.88±.04	.82±.04	.80±.04	.81±.05
	NeuroGPT-D	.88±.05	.82±.05	.82±.04	.85±.03
	BrainBERT	.74±.05	.69±.05	.61±.11	.57±.14
O	EEGPT	.96±.03	.91±.04	.90±.05	.89±.08
	NeuroLM	.82±.14	.75±.07	.74±.06	.77±.11

Table 13: Performance of BFM s on the ADHD-Child dataset.

Type	Model	AUROC	Acc	F1	F2
C	MBrain	.69±.11	.63±.08	.66±.06	.66±.04
	BIOT	.55±.05	.75±.06	.85±.04	.93±.02
	SppEEGNet	.53±.05	.49±.04	.48±.07	.45±.08
	Bendr	.53±.02	.51±.01	.52±.02	.49±.02
G	REVE	.79±.07	.71±.04	.74±.06	.74±.08
	BrainWave	.78±.04	.71±.04	.74±.06	.74±.12
	BrainOmni	.71±.09	.62±.07	.63±.09	.61±.14
	BFM	.69±.11	.69±.09	.75±.07	.75±.04
	LaBraM	.66±.12	.64±.08	.74±.06	.70±.07
	CBraMod	.64±.05	.64±.06	.73±.03	.81±.05
	Brant	.58±.07	.54±.07	.62±.15	.68±.23
	NeuroGPT-E	.55±.02	.56±.03	.72±.02	.86±.01
	BrainBERT	.55±.03	.56±.03	.56±.07	.53±.09
	NeuroGPT-D	.47±.12	.56±.06	.64±.11	.69±.18
O	EEGPT	.67±.13	.64±.10	.68±.10	.68±.12
	NeuroLM	.64±.06	.60±.05	.71±.04	.80±.05

Table 14: Performance of BFM s on the UCSD-OFF dataset.

Type	Model	AUROC	Acc	F1	F2
C	SppEEGNet	.53±.07	.51±.06	.59±.15	.71±.25
	Bendr	.52±.04	.51±.03	.48±.05	.47±.05
	BIOT	.51±.19	.49±.05	.56±.27	.69±.35
	MBrain	.50±.04	.44±.04	.32±.23	.34±.29
G	BrainOmni	.64±.09	.57±.06	.54±.16	.57±.26
	CBraMod	.63±.05	.58±.04	.46±.09	.40±.12
	REVE	.62±.19	.58±.17	.58±.19	.60±.24
	LaBraM	.59±.05	.56±.03	.57±.08	.60±.15
	BrainWave	.58±.06	.53±.10	.62±.12	.71±.19
	NeuroGPT-E	.56±.06	.54±.05	.57±.12	.62±.22
	BFM	.53±.03	.49±.12	.36±.09	.47±.17
	Brant	.52±.10	.45±.22	.42±.29	.58±.35
	BrainBERT	.51±.06	.54±.06	.49±.17	.49±.20
	NeuroGPT-D	.45±.07	.51±.05	.01±.01	.00±.01
O	EEGPT	.61±.13	.55±.08	.56±.10	.58±.17
	NeuroLM	.51±.07	.50±.05	.53±.15	.61±.23

Table 15: Performance of BFM s on the UCSD-ON dataset.

Type	Model	AUROC	Acc	F1	F2
C	Bendr	.51±.05	.49±.05	.43±.05	.41±.06
	SppEEGNet	.49±.08	.50±.11	.46±.23	.48±.27
	MBrain	.49±.15	.46±.14	.37±.17	.34±.18
	BIOT	.46±.18	.49±.05	.65±.05	.81±.04
G	BrainWave	.69±.20	.53±.08	.60±.06	.69±.14
	REVE	.63±.19	.56±.13	.45±.29	.46±.33
	CBraMod	.60±.12	.49±.08	.18±.08	.13±.07
	NeuroGPT-E	.56±.10	.53±.07	.58±.10	.64±.13
	Brant	.56±.11	.52±.11	.29±.28	.31±.34
	BrainOmni	.53±.14	.49±.12	.49±.16	.51±.20
	LaBraM	.51±.22	.45±.11	.33±.19	.31±.19
	BrainBERT	.51±.05	.51±.06	.51±.11	.54±.17
	NeuroGPT-D	.46±.10	.47±.06	.29±.25	.31±.28
	BFM	.44±.08	.48±.07	.42±.17	.42±.20
O	EEGPT	.51±.21	.48±.17	.49±.15	.49±.14
	NeuroLM	.44±.18	.51±.18	.47±.24	.48±.29

Table 16: Performance of BFM_s on the EEGMat dataset.

Type	Model	AUROC	Acc	F1	F2
C	MBrain	.68±.06	.75±.02	.13±.15	.10±.11
	BIOT	.59±.08	.27±.01	.42±.01	.65±.01
	Bendr	.54±.02	.66±.05	.34±.07	.34±.06
	SppEEGNet	.52±.03	.50±.07	.37±.04	.47±.09
G	REVE	.78±.09	.75±.08	.39±.27	.61±.09
	LaBraM	.71±.03	.68±.04	.48±.07	.53±.13
	NeuroGPT-E	.70±.04	.73±.04	.25±.20	.22±.20
	BrainOmni	.68±.07	.60±.07	.48±.04	.60±.06
	BrainWave	.66±.06	.51±.20	.44±.07	.55±.08
	CBraMod	.63±.06	.72±.04	.19±.18	.16±.17
	BrainBERT	.61±.07	.67±.06	.45±.09	.50±.13
	BFM	.60±.03	.66±.04	.35±.06	.36±.10
	Brant	.57±.12	.75±.01	.00±.00	.00±.00
	NeuroGPT-D	.51±.06	.73±.01	.00±.00	.00±.00
O	EEGPT	.67±.04	.64±.06	.49±.02	.59±.04
	NeuroLM	.63±.08	.31±.10	.42±.04	.64±.04

Table 17: Performance of BFM_s on the SD-28 dataset.

Type	Model	AUROC	Acc	F1	F2
C	MBrain	.58±.10	.58±.10	.64±.13	.66±.15
	BIOT	.56±.09	.62±.12	.68±.18	.65±.21
	Bendr	.49±.05	.50±.03	.48±.05	.45±.04
	SppEEGNet	.49±.03	.47±.04	.33±.06	.27±.05
G	BrainWave	.88±.07	.81±.06	.83±.08	.81±.11
	REVE	.81±.13	.75±.13	.80±.10	.86±.11
	NeuroGPT-D	.80±.17	.77±.13	.80±.11	.84±.14
	BrainBERT	.73±.11	.66±.15	.63±.26	.62±.29
	NeuroGPT-E	.72±.12	.66±.14	.73±.15	.69±.19
	BrainOmni	.69±.15	.69±.12	.73±.14	.77±.19
	BFM	.69±.15	.62±.05	.73±.04	.81±.08
	CBraMod	.54±.14	.58±.05	.58±.18	.58±.24
	LaBraM	.54±.07	.54±.04	.59±.07	.59±.13
	Brant	.51±.11	.46±.08	.47±.17	.50±.30
O	EEGPT	.56±.21	.56±.11	.62±.12	.66±.15
	NeuroLM	.49±.04	.49±.05	.53±.28	.62±.35

Table 18: Performance of BFM_s on the MDD-64 dataset.

Type	Model	AUROC	Acc	F1	F2
C	MBrain	.93±.08	.87±.11	.89±.08	.91±.05
	Bendr	.78±.07	.73±.04	.75±.03	.76±.04
	BIOT	.53±.12	.33±.01	.50±.01	.71±.00
	SppEEGNet	.52±.02	.55±.04	.50±.05	.45±.05
G	REVE	.97±.04	.88±.09	.90±.06	.92±.04
	BrainOmni	.94±.07	.85±.09	.87±.07	.89±.05
	BrainWave	.94±.03	.85±.02	.84±.03	.81±.06
	BFM	.93±.08	.86±.11	.88±.08	.91±.05
	BrainBERT	.92±.07	.85±.07	.85±.06	.85±.10
	Brant	.92±.09	.80±.10	.80±.14	.80±.19
	CBraMod	.90±.13	.84±.12	.86±.09	.87±.09
	LaBraM	.87±.12	.81±.11	.78±.09	.83±.04
	NeuroGPT-E	.87±.05	.80±.05	.84±.03	.90±.03
	NeuroGPT-D	.70±.12	.67±.13	.77±.07	.89±.04
O	EEGPT	.94±.05	.87±.08	.88±.06	.90±.04
	NeuroLM	.82±.11	.80±.06	.80±.09	.81±.18

Table 19: Performance of BFM_s on the Dep-BDI dataset.

Type	Model	AUROC	Acc	F1	F2
C	BIOT	.60±.11	.30±.17	.11±.02	.22±.05
	MBrain	.59±.07	.62±.03	.24±.16	.20±.16
	Bendr	.54±.03	.54±.03	.45±.03	.47±.03
	SppEEGNet	.50±.02	.49±.04	.41±.04	.45±.04
G	BrainWave	.72±.03	.66±.03	.62±.03	.67±.06
	BrainOmni	.68±.12	.63±.09	.55±.10	.58±.13
	REVE	.67±.12	.65±.08	.47±.14	.45±.17
	LaBraM	.65±.10	.59±.11	.60±.09	.71±.08
	BrainBERT	.64±.09	.61±.05	.48±.11	.48±.12
	BFM	.62±.10	.59±.06	.48±.10	.51±.13
	NeuroGPT-E	.59±.08	.62±.01	.02±.02	.01±.01
	CBraMod	.54±.05	.69±.14	.13±.08	.16±.10
	Brant	.53±.09	.62±.01	.00±.00	.00±.00
	NeuroGPT-D	.51±.08	.62±.01	.00±.00	.00±.00
O	EEGPT	.63±.04	.62±.05	.50±.05	.51±.11
	NeuroLM	.54±.05	.61±.02	.30±.26	.31±.31

Table 20: Performance of BFM_s on the Dep-STAI dataset.

Type	Model	AUROC	Acc	MF1	Kappa
C	BIOT	.56±.09	.37±.07	.33±.07	.073±.088
	MBrain	.55±.04	.60±.03	.30±.05	.054±.059
	Bendr	.54±.03	.48±.03	.36±.03	.047±.041
	SppEEGNet	.51±.02	.46±.03	.33±.01	.007±.024
G	BrainWave	.64±.06	.51±.05	.42±.05	.150±.053
	NeuroGPT-E	.61±.09	.55±.07	.38±.10	.129±.155
	LaBraM	.61±.09	.36±.10	.26±.06	.081±.093
	BrainBERT	.60±.06	.48±.11	.32±.08	.064±.126
	BrainOmni	.60±.06	.53±.05	.36±.05	.105±.062
	BFM	.58±.08	.45±.09	.37±.06	.099±.117
	NeuroGPT-D	.57±.06	.61±.01	.25±.00	.000±.000
	REVE	.54±.11	.54±.10	.35±.08	.079±.200
	CBraMod	.54±.04	.60±.02	.30±.04	.049±.052
	Brant	.53±.03	.61±.01	.25±.00	.000±.000
O	EEGPT	.56±.06	.51±.06	.34±.06	.025±.080
	NeuroLM	.50±.04	.58±.04	.26±.02	.009±.018

Table 21: Performance of BFM_s on the ISRUC-G1 dataset.

Type	Model	AUROC	Acc	MF1	Kappa
C	MBrain	.87±.04	.63±.07	.55±.07	.514±.084
	BIOT	.78±.04	.46±.07	.44±.02	.322±.071
	Bendr	.72±.04	.43±.07	.39±.05	.269±.076
	SppEEGNet	.53±.01	.17±.03	.15±.02	.012±.009
G	REVE	.92±.01	.69±.03	.65±.05	.598±.036
	BrainOmni	.91±.02	.68±.03	.64±.04	.581±.030
	BrainWave	.89±.01	.62±.05	.60±.02	.522±.064
	CBraMod	.86±.05	.54±.08	.48±.10	.419±.094
	LaBraM	.85±.02	.61±.02	.56±.05	.502±.028
	Brant	.84±.02	.55±.01	.50±.04	.427±.016
	NeuroGPT-E	.80±.02	.44±.11	.41±.11	.319±.101
	BrainBERT	.80±.03	.47±.05	.42±.07	.332±.058
	BFM	.78±.03	.47±.04	.37±.13	.264±.148
	NeuroGPT-D	.61±.07	.31±.07	.17±.08	.060±.102
O	EEGPT	.87±.02	.60±.05	.57±.08	.486±.070
	NeuroLM	.67±.05	.27±.11	.15±.10	.074±.074

Table 22: Performance of BFM on the SleepEDF dataset.

Type	Model	AUROC	Acc	MF1	Kappa
C	MBrain	.94±.01	.79±.04	.73±.05	.709±.059
	Bendr	.91±.01	.69±.06	.65±.04	.591±.062
	BIOT	.58±.16	.35±.16	.21±.12	.070±.145
	SppEEGNet	.57±.01	.22±.01	.20±.01	.104±.028
G	NeuroGPT-E	.94±.01	.78±.03	.70±.03	.696±.045
	Brant	.94±.01	.73±.07	.70±.05	.639±.083
	CBraMod	.93±.01	.73±.04	.69±.04	.642±.054
	LaBraM	.93±.01	.76±.04	.68±.03	.669±.050
	BrainBERT	.91±.02	.68±.07	.65±.05	.578±.079
	BrainWave	.89±.02	.67±.05	.54±.08	.516±.104
	BFM	.89±.01	.65±.04	.60±.03	.558±.053
	BrainOmni	.87±.00	.63±.03	.60±.01	.506±.025
	REVE	.78±.38	.63±.30	.60±.28	.561±.257
	NeuroGPT-D	.65±.03	.48±.04	.21±.05	.100±.068
O	EEGPT	.91±.00	.68±.03	.66±.01	.578±.026
	NeuroLM	.61±.06	.18±.04	.11±.03	.189±.263

Table 23: Performance of BFM on the BCI-2a dataset.

Type	Model	AUROC	Acc	MF1	Kappa
C	MBrain	.54±.02	.27±.02	.19±.03	.027±.023
	Bendr	.51±.01	.25±.01	.25±.01	.005±.011
	SppEEGNet	.51±.01	.25±.01	.24±.02	.003±.020
	BIOT	.50±.01	.24±.02	.17±.02	-.015±.022
G	REVE	.61±.01	.34±.01	.30±.02	.115±.012
	NeuroGPT-E	.61±.02	.35±.03	.33±.02	.128±.041
	LaBraM	.55±.03	.28±.02	.23±.04	.045±.027
	Brant	.54±.00	.25±.00	.10±.00	.000±.000
	BrainWave	.54±.02	.27±.02	.20±.03	.031±.022
	BrainOmni	.54±.01	.27±.02	.22±.02	.021±.029
	CBraMod	.54±.01	.27±.01	.20±.02	.022±.012
	BFM	.51±.01	.26±.01	.25±.00	.013±.012
	NeuroGPT-D	.51±.03	.26±.01	.15±.03	.007±.019
	BrainBERT	.50±.01	.25±.02	.23±.02	.005±.023
O	EEGPT	.57±.03	.28±.02	.22±.01	.036±.024
	NeuroLM	.52±.02	.27±.01	.20±.02	.030±.018

Table 24: Performance of BFM on the EEGMMIDB-I dataset.

Type	Model	AUROC	Acc	MF1	Kappa
C	Bendr	.55±.01	.29±.01	.29±.01	.054±.010
	MBrain	.51±.01	.26±.01	.16±.05	.009±.011
	SppEEGNet	.51±.01	.26±.01	.23±.01	.008±.013
	BIOT	.50±.01	.25±.00	.20±.02	-.005±.004
G	REVE	.82±.01	.59±.02	.59±.02	.451±.031
	NeuroGPT-E	.78±.01	.54±.01	.54±.01	.392±.019
	BrainOmni	.76±.01	.51±.01	.51±.01	.351±.019
	LaBraM	.59±.02	.31±.02	.25±.03	.078±.032
	CBraMod	.58±.02	.30±.02	.28±.04	.073±.028
	BFM	.52±.01	.27±.01	.26±.01	.023±.009
	BrainWave	.51±.01	.25±.01	.18±.01	.001±.014
	Brant	.51±.01	.25±.00	.10±.00	.000±.000
	BrainBERT	.49±.00	.25±.00	.16±.02	-.003±.005
	NeuroGPT-D	.49±.01	.25±.01	.16±.05	-.007±.008
O	EEGPT	.52±.01	.27±.02	.24±.04	.023±.022
	NeuroLM	.51±.01	.25±.01	.15±.05	.005±.008

Table 25: Performance of BFM on the EEGMMIDB-R dataset.

Type	Model	AUROC	Acc	MF1	Kappa
C	Bendr	.55±.01	.29±.01	.29±.01	.060±.014
	SppEEGNet	.52±.00	.26±.01	.24±.01	.014±.008
	MBrain	.52±.01	.26±.01	.19±.05	.008±.016
	BIOT	.50±.01	.25±.01	.21±.02	.003±.011
G	REVE	.82±.00	.59±.01	.58±.01	.448±.014
	NeuroGPT-E	.77±.02	.54±.02	.53±.02	.381±.030
	BrainOmni	.74±.01	.49±.01	.49±.01	.325±.014
	CBraMod	.57±.01	.30±.02	.27±.03	.061±.022
	LaBraM	.55±.02	.28±.02	.23±.03	.041±.027
	BFM	.52±.01	.27±.01	.26±.01	.024±.008
	NeuroGPT-D	.50±.00	.25±.00	.14±.01	.003±.003
	Brant	.50±.01	.25±.00	.10±.00	.000±.000
	BrainWave	.50±.01	.25±.01	.17±.02	-.004±.011
	BrainBERT	.50±.01	.25±.00	.16±.03	.001±.006
O	NeuroLM	.52±.02	.26±.01	.14±.05	.009±.017
	EEGPT	.51±.01	.25±.01	.23±.03	.006±.017

Table 26: Performance of BFM on the DEAP dataset.

Type	Model	AUROC	Acc	MF1	Kappa
C	SppEEGNet	.51±.03	.27±.06	.23±.03	.007±.027
	MBrain	.51±.05	.42±.04	.15±.01	.000±.000
	BIOT	.50±.03	.30±.06	.18±.02	-.014±.030
	Bendr	.50±.02	.26±.02	.24±.02	-.004±.035
G	BrainBERT	.52±.02	.23±.02	.18±.03	.017±.020
	NeuroGPT-D	.51±.03	.44±.04	.15±.01	.000±.000
	BrainWave	.51±.03	.27±.07	.23±.06	.010±.077
	CBraMod	.51±.01	.19±.02	.14±.02	-.001±.009
	LaBraM	.51±.02	.29±.04	.21±.03	.016±.014
	REVE	.50±.05	.26±.05	.21±.03	-.013±.035
	BFM	.50±.02	.28±.07	.22±.02	.005±.015
	NeuroGPT-E	.49±.01	.42±.03	.17±.03	-.004±.006
	Brant	.48±.02	.34±.17	.12±.06	.000±.000
	BrainOmni	.45±.03	.22±.03	.19±.01	-.046±.022
O	NeuroLM	.51±.03	.33±.13	.13±.03	-.003±.007
	EEGPT	.50±.02	.26±.05	.22±.04	.029±.027

Table 27: Performance of BFM on the SEED-IV dataset.

Type	Model	AUROC	Acc	MF1	Kappa
C	MBrain	.52±.01	.26±.01	.21±.04	.014±.020
	Bendr	.50±.00	.25±.00	.25±.00	-.001±.005
	SppEEGNet	.50±.00	.25±.00	.24±.00	-.001±.002
	BIOT	.48±.00	.24±.01	.19±.02	-.018±.003
G	NeuroGPT-E	.57±.01	.30±.01	.26±.02	.003±.005
	REVE	.54±.01	.28±.02	.27±.01	.039±.019
	BrainOmni	.53±.01	.28±.02	.26±.01	.035±.019
	BrainWave	.53±.02	.27±.02	.22±.03	.023±.026
	BFM	.52±.01	.27±.01	.24±.01	.012±.004
	CBraMod	.51±.01	.26±.01	.21±.03	.010±.010
	BrainBERT	.51±.03	.25±.02	.17±.05	.003±.012
	LaBraM	.51±.01	.25±.01	.20±.02	.008±.014
	NeuroGPT-D	.50±.00	.27±.00	.11±.00	.000±.000
	Brant	.50±.01	.26±.01	.10±.00	.000±.000
O	EEGPT	.51±.01	.25±.01	.22±.02	.006±.016
	NeuroLM	.50±.00	.25±.00	.13±.04	.001±.002

Table 28: Performance of BFM on the Chisco-I dataset.

Type	Model	AUROC	Acc	MF1	Kappa
C	MBrain	.50±.01	.03±.00	.00±.00	.000±.001
	Bendr	.50±.01	.03±.00	.02±.00	.000±.002
	SppEEGNet	.50±.00	.02±.00	.01±.00	-.000±.001
	BIOT	.49±.00	.03±.01	.01±.00	.000±.001
G	LaBraM	.51±.01	.04±.01	.01±.00	.005±.004
	CBraMod	.51±.01	.04±.01	.01±.00	.003±.003
	BrainOmni	.50±.01	.02±.00	.01±.00	.001±.001
	BFM	.50±.00	.03±.00	.01±.00	.001±.001
	NeuroGPT-D	.50±.00	.05±.00	.00±.00	.001±.004
	BrainBERT	.50±.01	.03±.00	.01±.01	.001±.003
	REVE	.50±.00	.03±.00	.02±.00	.000±.001
	NeuroGPT-E	.50±.01	.05±.00	.00±.00	-.000±.004
	BrainWave	.50±.01	.03±.01	.00±.00	.002±.003
	Brant	.50±.00	.04±.01	.00±.00	.000±.000
O	EEGPT	.50±.00	.03±.01	.01±.00	.001±.003
	NeuroLM	.50±.00	.04±.01	.00±.00	-.001±.001

Table 29: Performance of BFM on the Chisco-R dataset.

Type	Model	AUROC	Acc	MF1	Kappa
C	BIOT	.50±.01	.04±.00	.01±.00	-.000±.003
	MBrain	.50±.00	.04±.00	.00±.00	.000±.000
	SppEEGNet	.50±.00	.02±.00	.01±.00	.000±.003
	Bendr	.50±.00	.03±.00	.02±.00	.001±.003
G	BrainWave	.51±.02	.03±.01	.00±.00	.001±.003
	BrainOmni	.51±.01	.03±.01	.01±.00	.002±.005
	LaBraM	.51±.01	.03±.01	.01±.00	.002±.004
	NeuroGPT-D	.51±.01	.05±.00	.00±.00	.002±.003
	CBraMod	.51±.01	.03±.01	.01±.00	-.000±.005
	NeuroGPT-E	.50±.01	.05±.00	.00±.00	.001±.003
	BFM	.50±.00	.03±.01	.01±.00	.001±.002
	REVE	.50±.01	.03±.00	.02±.00	.000±.003
	Brant	.50±.00	.04±.01	.00±.00	.000±.000
	BrainBERT	.50±.00	.03±.01	.00±.00	.001±.001
O	EEGPT	.50±.01	.03±.01	.01±.01	.002±.002
	NeuroLM	.50±.00	.03±.02	.00±.00	-.000±.000

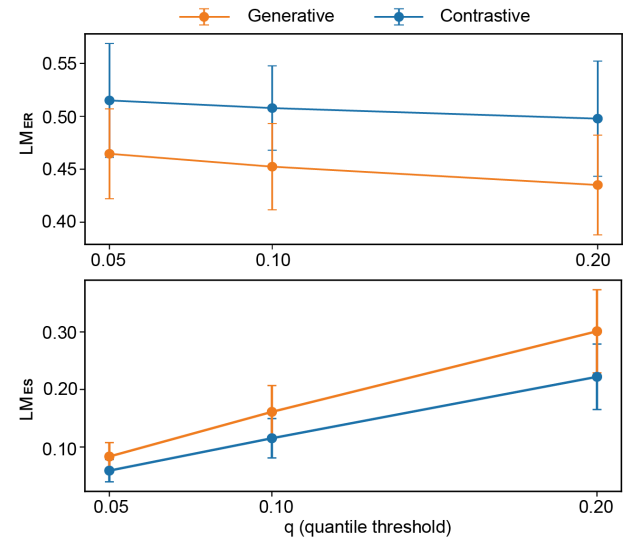
E Additional Results for SSL Strategy Analysis

This section reports full results and robustness checks that support the trends discussed in Section 3.3.2. Specifically, we report the complete quantitative results of the decision-boundary and embedding diagnostics across all evaluated models, and a sensitivity analysis with respect to the boundary quantile parameter q . Table 30 reports the decision-boundary metrics LM_{ER} and LM_{ES} and the embedding class-separation ratio R_{cls} for all contrastive- and generative-based BFM on the three representative datasets analyzed in the main text. The complete table allows a fine-grained comparison beyond the representative models shown in the main paper.

Figure 4 presents a sensitivity analysis of the decision-boundary metrics under different quantile thresholds $q \in \{0.05, 0.10, 0.20\}$ used to define the low-margin region \mathcal{B}_q . While absolute values vary with q , the relative trends between contrastive and generative models remain stable. This confirms that the conclusions are not an artifact of a specific boundary choice.

Table 30: Full quantitative results of decision-boundary diagnostics. The table reports LM_{ER} , LM_{ES} , and R_{cls} for all contrastive- and generative-based models ($q=0.10$).

Model	ADFD			CHBMIT			SD-28		
	LM_{ER}	LM_{ES}	R_{cls}	LM_{ER}	LM_{ES}	R_{cls}	LM_{ER}	LM_{ES}	R_{cls}
SppEEGNet	.497	.107	0.658	.483	.127	2.208	.490	.098	1.557
Bendr	.499	.105	0.658	.497	.117	0.962	.488	.094	0.941
BIOT	.470	.098	2.344	.615	.087	2.328	.497	.112	2.865
MBrain	.526	.113	1.980	.550	.219	2.047	.480	.103	2.590
BrainBERT	.492	.126	0.842	.457	.203	2.103	.478	.157	2.091
BrainWave	.455	.172	2.275	.499	.197	2.613	.409	.179	3.229
CBraMod	.492	.109	1.892	.445	.161	2.207	.456	.097	2.510
BrainOmni	.487	.175	3.465	.469	.173	2.558	.376	.122	3.546
REVE	.431	.205	2.914	.447	.261	2.408	.447	.213	3.534
NeuroGPT-E	.506	.193	3.736	.478	.201	3.385	.422	.219	5.577
LaBraM	.443	.176	3.846	.435	.179	2.979	.482	.098	2.003
BFM	.490	.124	0.815	.460	.169	0.838	.516	.134	1.266
Brant	.408	.089	0.730	.361	.146	0.791	.375	.070	1.551

**Figure 4:** Sensitivity of decision-boundary error concentration to the boundary definition.

F Additional Spatial Analysis Results

This appendix provides detailed results supporting the spatial-structure analysis discussed in Section 3.3.3. We report the full quantitative impact of channel-permutation perturbations across datasets and models. We permute channels in the training and validation splits to probe whether BFM encode dataset-specific spatial structure. All other settings are kept identical, so any performance change is attributable to disrupted channel topology. Tables 31 to 34 reports all metrics before or after permutation. We focus on AUROC in the main analysis, and these results support that some BFM internalize dataset-specific spatial structure during training.

Table 31: Performance under channel-permutation setting. We report AUROC, Accuracy, F1 and F2 for models trained on original data (origin) and shuffled data (shuffle) on ADHD-Child.

	AUROC	Acc	F1	F2				
Model	shuffle	origin	shuffle	origin	shuffle	origin	shuffle	origin
BrainBERT	.54±.04	.55±.03	.55±.03	.56±.03	.58±.04	.56±.07	.58±.05	.53±.09
BrainWave	.68±.04	.78±.04	.66±.05	.71±.04	.68±.12	.74±.06	.68±.19	.74±.12
BrainOmni	.71±.09	.71±.09	.62±.07	.62±.07	.63±.09	.63±.09	.61±.15	.61±.14
CBraMod	.60±.06	.64±.05	.57±.03	.64±.06	.72±.03	.73±.03	.85±.03	.81±.05
EEGPT	.63±.11	.67±.13	.60±.10	.64±.10	.57±.28	.68±.10	.59±.32	.68±.12
MBrain	.69±.11	.69±.11	.63±.09	.63±.08	.68±.07	.66±.06	.70±.05	.66±.04
NeuroGPT-E	.55±.02	.55±.02	.56±.03	.56±.03	.72±.02	.72±.02	.86±.01	.86±.01
REVE	.71±.09	.79±.07	.55±.11	.71±.04	.36±.31	.74±.06	.32±.30	.74±.08

Table 32: Channel-permutation setting performance on ADFD.

	AUROC	Acc	F1	F2				
Model	shuffle	origin	shuffle	origin	shuffle	origin	shuffle	origin
BrainBERT	.62±.05	.59±.05	.64±.01	.58±.05	.66±.02	.60±.11	.64±.04	.64±.15
BrainWave	.62±.12	.74±.05	.57±.09	.68±.05	.49±.26	.68±.10	.47±.31	.73±.10
BrainOmni	.80±.07	.80±.07	.71±.04	.71±.04	.73±.05	.73±.05	.72±.09	.72±.09
CBraMod	.51±.02	.55±.06	.52±.07	.59±.04	.32±.26	.41±.20	.28±.25	.37±.20
EEGPT	.79±.04	.81±.05	.72±.05	.72±.05	.72±.05	.73±.05	.68±.07	.70±.07
MBrain	.52±.13	.53±.12	.51±.09	.50±.10	.54±.12	.53±.12	.54±.15	.52±.14
NeuroGPT-E	.49±.05	.51±.03	.55±.01	.55±.01	.71±.01	.71±.01	.85±.01	.85±.01
REVE	.79±.08	.84±.07	.68±.07	.77±.08	.74±.05	.79±.07	.79±.07	.79±.09

Table 33: Channel-permutation setting performance on CHBMIT.

	AUROC	Acc	F1	F2				
Model	shuffle	origin	shuffle	origin	shuffle	origin	shuffle	origin
BrainBERT	.79±.04	.78±.06	.80±.04	.75±.10	.59±.08	.58±.11	.59±.11	.61±.09
BrainWave	.59±.14	.90±.03	.63±.09	.80±.12	.30±.11	.71±.09	.32±.15	.78±.04
BrainOmni	.74±.13	.74±.13	.67±.19	.67±.19	.51±.12	.51±.12	.56±.12	.56±.12
CBraMod	.67±.12	.69±.04	.67±.11	.70±.08	.42±.16	.46±.08	.48±.23	.49±.14
EEGPT	.69±.13	.71±.09	.73±.10	.67±.11	.47±.16	.46±.06	.48±.19	.51±.15
MBrain	.70±.08	.71±.03	.77±.03	.73±.06	.22±.22	.31±.15	.17±.18	.28±.20
NeuroGPT-E	.65±.07	.78±.12	.70±.06	.75±.07	.26±.10	.51±.22	.24±.14	.63±.16
REVE	.78±.12	.84±.10	.59±.25	.78±.12	.53±.18	.63±.14	.65±.12	.66±.13

Table 34: Channel-permutation setting performance on UCSD-ON.

	AUROC	Acc	F1	F2				
Model	shuffle	origin	shuffle	origin	shuffle	origin	shuffle	origin
BrainBERT	.50±.09	.51±.05	.49±.05	.51±.06	.57±.04	.51±.11	.64±.06	.54±.17
BrainWave	.50±.11	.69±.10	.49±.12	.53±.08	.40±.28	.60±.06	.43±.31	.69±.14
BrainOmni	.51±.19	.64±.09	.46±.15	.57±.06	.44±.21	.54±.16	.46±.26	.57±.26
CBraMod	.59±.08	.60±.12	.51±.07	.49±.08	.21±.29	.18±.08	.22±.35	.13±.07
EEGPT	.63±.17	.51±.21	.55±.14	.48±.17	.49±.16	.49±.15	.46±.16	.49±.14
MBrain	.43±.16	.49±.15	.46±.06	.46±.14	.49±.21	.37±.17	.56±.28	.34±.18
NeuroGPT-E	.55±.25	.56±.10	.53±.10	.53±.07	.51±.25	.58±.10	.57±.34	.64±.13
REVE	.58±.12	.63±.19	.58±.06	.56±.13	.53±.17	.45±.29	.53±.25	.46±.33

Table 35: Channel-permutation performance on UCSD-OFF.

Model	AUROC		Acc		F1		F2	
	shuffle	origin	shuffle	origin	shuffle	origin	shuffle	origin
BrainBERT	.52±.09	.51±.06	.53±.06	.54±.06	.60±.10	.49±.17	.68±.15	.49±.20
BrainWave	.49±.19	.58±.06	.56±.10	.53±.10	.43±.29	.62±.12	.44±.34	.71±.19
BrainOmni	.62±.07	.64±.09	.56±.04	.57±.06	.57±.10	.54±.16	.61±.21	.57±.26
CBraMod	.60±.05	.63±.05	.56±.04	.58±.04	.32±.17	.46±.09	.27±.19	.40±.12
EEGPT	.62±.15	.61±.13	.60±.12	.55±.08	.55±.17	.56±.10	.53±.20	.58±.17
MBrain	.48±.09	.50±.04	.44±.06	.44±.04	.35±.22	.32±.23	.38±.31	.34±.29
NeuroGPT-E	.56±.07	.56±.06	.52±.05	.54±.05	.57±.09	.57±.12	.63±.17	.62±.22
REVE	.63±.11	.62±.19	.59±.13	.58±.17	.61±.13	.58±.19	.63±.16	.60±.24

G Additional Frequency Analysis Results

This appendix provides detailed results supporting the frequency-band analysis described in Section 3.3.4. We report the full quantitative outcomes of the band-wise PSD prediction experiments. Tables 36 to 38 reports the band-wise prediction performance for all evaluated models across the six canonical frequency bands. For each band b , we list the correlation between the ground-truth PS and the predicted PSD, as well as the normalized relative strength r_b^n used in the main analysis.

Table 36: Band-wise PSD predictability across BFM on ADFD and Dep-122, reporting normalized band predictability r_b^n for delta (d), theta (t), alpha (a), beta (b), low gamma (gl), and high gamma (gh).

Model	ADFD						Dep-122					
	r_d^n	r_t^n	r_a^n	r_b^n	r_{gl}^n	r_{gh}^n	r_d^n	r_t^n	r_a^n	r_b^n	r_{gl}^n	r_{gh}^n
REVE	.85	.00	.71	.11	.59	1.0	.99	.00	1.0	.92	.78	.65
EEGPT	1.0	.32	.36	.20	.92	.00	.80	.67	1.0	.67	.13	.00
BrainOmni	.95	.00	.82	.02	.28	1.0	.83	.39	1.0	.81	.35	.00
BrainWave	.63	.35	.77	.00	.14	1.0	1.0	.47	.75	.23	.00	.28
LaBraM	.08	.00	1.0	.26	.28	.10	.77	.36	1.0	.55	.15	.00
BrainBERT	.69	.08	.16	.00	.68	1.0	.70	.44	1.0	.00	.27	.87
BFM	.89	.00	.33	.09	.27	1.0	.89	1.0	.99	.76	1.0	.71
BIOT	.87	.00	.62	.31	.37	1.0	.80	.38	1.0	.75	.17	.00
CBraMod	.84	.00	.67	.55	.64	1.0	.91	.00	1.0	.86	.47	.05
MBrain	.87	.00	.42	.15	.40	1.0	.98	.00	1.0	.87	.87	.61
SppEEGNet	.26	.10	.00	.02	.27	1.0	1.0	.55	.94	.27	.00	.08
NeuroLM	.66	.89	.51	.08	.00	1.0	1.0	.36	.35	.00	.20	.05
NeuroGPT-E	.85	.13	.00	.01	.06	1.0	.52	.39	1.0	.00	.06	.10
Bendr	.74	.28	.00	.10	.07	1.0	1.0	.28	.79	.44	.00	.03
Brant	.53	.33	.17	.08	.00	1.0	.00	.68	.33	.43	.93	1.0
NeuroGPT-D	.95	.23	.25	.10	.00	1.0	1.0	.30	.86	.62	.11	.00

Table 37: Band-wise PSD predictability on SD-8 and MDD-64.

Model	SD-28						MDD-64					
	r_d^n	r_t^n	r_a^n	r_b^n	r_{gl}^n	r_{gh}^n	r_d^n	r_t^n	r_a^n	r_b^n	r_{gl}^n	r_{gh}^n
BrainWave	.95	.64	1.0	.75	.00	.22	.89	1.0	.89	.61	.00	.02
REVE	1.0	.00	.97	.66	.67	.22	.96	1.0	.99	1.0	.93	.00
NeuroGPT-E	1.0	.87	.06	.00	.41	.90	.25	1.0	.00	.62	.60	.08
BrainBERT	.82	.15	1.0	.00	.13	.29	.75	1.0	.73	.70	.80	.00
BrainOmni	.86	.46	1.0	.71	.27	.00	.66	.84	1.0	.99	.74	.00
BFM	.92	.00	1.0	.84	.90	.84	.86	1.0	.97	.97	.97	.00
MBrain	1.0	.00	1.0	.94	.83	.69	.94	.96	.96	1.0	.92	.00
EEGPT	.91	.66	1.0	.97	.38	.00	.89	.97	1.0	.89	.74	.00
BIOT	.68	.00	1.0	.58	.65	.19	.93	.97	1.0	.99	.86	.00
NeuroGPT-D	1.0	.00	.76	.67	.36	.14	.92	1.0	.98	.71	.67	.00
CBraMod	1.0	.25	.90	.89	.58	.00	.95	.96	.98	1.0	.90	.00
LaBraM	.87	.44	1.0	.70	.34	.00	.59	.86	.59	1.0	.76	.00
Brant	.64	.00	1.0	.71	.61	.54	.84	.87	.89	1.0	.93	.00
Bendr	1.0	.34	.53	.51	.01	.00	.73	1.0	.48	.49	.46	.00
SppEEGNet	1.0	.16	.68	.29	.00	.02	1.0	.84	.78	.63	.51	.00
NeuroLM	1.0	.31	.81	.31	.00	.24	.59	.86	.59	1.0	.76	.00

Table 38: Band-wise PSD predictability across BFM on ADHD.

Model	ADHD-Adult						ADHD-Child					
	r_d^n	r_t^n	r_a^n	r_b^n	r_{gl}^n	r_{gh}^n	r_d^n	r_t^n	r_a^n	r_b^n	r_{gl}^n	r_{gh}^n
EEGPT	.66	.00	.59	1.0	.18	.08	.95	.82	1.0	1.0	.56	.00
BrainOmni	.65	.00	.67	1.0	.32	.14	1.0	.86	.99	.84	.39	.00
BrainWave	.32	.00	.68	1.0	.80	.82	.83	.59	.94	1.0	.34	.00
BIOT	.40	.00	.40	1.0	.58	.17	.98	.89	1.0	.78	.32	.00
REVE	.71	.00	.25	1.0	.53	.30	.96	.82	.98	1.0	.62	.00
MBrain	.66	.00	.55	1.0	.53	.16	1.0	.87	.98	1.0	.60	.00
Brant	.71	.00	.33	1.0	.32	.08	.89	.58	.68	1.0	.59	.00
CBraMod	.65	.19	.61	1.0	.52	.00	.99	.86	.94	1.0	.79	.00
LaBraM	.76	.39	.71	1.0	.08	.00	1.0	.86	.96	.92	.41	.00
NeuroGPT-E	.39	.74	.00	1.0	.40	.15	.84	1.0	.75	.37	.00	.44
NeuroGPT-D	.95	.00	.71	1.0	.16	.03	1.0	.70	.83	.77	.34	.00
BFM	.61	.00	.45	1.0	.70	.62	.96	.83	.94	1.0	.67	.00
NeuroLM	.41	.00	.55	1.0	.29	.19	1.0	.82	.97	.88	.27	.00
BrainBERT	1.0	.26	.91	.84	.13	.00	1.0	.64	.82	.66	.60	.00
SppEEGNet	1.0	.06	.72	.61	.06	.00	1.0	.80	.70	.64	.31	.00
Bendr	1.0	.16	.73	.78	.03	.00	1.0	.62	.83	.57	.20	.00

H Additional Codebook Analysis Results

This section complements the codebook analysis discussed of LaBraM in Section 3.3.5. LaBraM adopts a discrete codebook during pre-training. However, in its standard downstream finetuning protocol, it finetunes the encoder and task head while keeping the codebook unused (i.e., finetuning is performed on continuous embeddings). To isolate the effect of reusing discretization at finetuning time, we additionally evaluate a variant that enables codebook-based finetuning (CB) and compare it against the standard setting (origin) on four representative datasets, with all other settings held fixed. Table 40 reports full results for both variants. LaBraM codebook analysis on ADFD, CHBMIT, SleepEDF, and SD-28. We report AUROC, Accuracy, F1, and F2 for the binary datasets, and AUROC (OvR), Accuracy, MF1, and Cohen’s κ for SleepEDF.

Table 39: LaBraM codebook analysis on ADFD, CHBMIT, and SD-28. We compare standard finetuning without codebook (Origin) and codebook-enabled finetuning (CB) under identical protocols, reporting AUROC, Accuracy, F1, and F2.

Dataset	AUROC		Acc		F1		F2	
	CB	origin	CB	origin	CB	origin	CB	origin
ADFD	.65±.06	.77±.10	.62±.05	.72±.08	.68±.03	.75±.06	.70±.03	.75±.06
CHBMIT	.77±.06	.78±.07	.75±.04	.75±.06	.60±.10	.54±.24	.55±.7	.53±.16
SD-28	.47±.12	.54±.07	.50±.09	.54±.04	.56±.12	.59±.07	.60±.15	.59±.13

Table 40: LaBraM codebook analysis on SleepEDF, reporting Accuracy, AUROC (OvR), macro-F1 (MF1), and Cohen’s κ .

CB	AUROC		Acc		MF1		Kappa	
	origin	CB	origin	CB	origin	CB	origin	CB
.86±.02	.93±.01	.66±.04	.76±.04	.61±.03	.68±.03	.54±.05	.67±.05	